Supporting information

Charge pumping enabling Co-NC to outperform benchmark Pt catalyst for pH-universal hydrogen evolution reaction

Ziliang Chen,[‡,a,b] Huilin Qing,[‡,a] Ruirui Wang[a] and Renbing Wu*[,a]

[a] Department of Materials Science, Fudan University, Shanghai 200433, China

[b] Institute of Functional Nano & Soft Materials (FUNSOM), Soochow University, Suzhou 215123, China

‡ Z. Chen and H. Qing contributed equally in this work.

*Email: rbwu@fudan.edu.cn

Table S1. The amount of Zn in NC before and after acid leaching treatment.

Element in sample	**Amount (wt.%)**
Zn in NC before leaching	3.5
Zn in NC after leaching	0.2

Table S2. Structural parameters and phase abundance for VN/Co-NC, VN-NC, Co-NC, VN/Co-NC-4, and VN/Co-NC-8 samples refined from the experimental XRD profiles.

Sample	Phase	Space group	Lattice parameters (Å)			Abundance
			a	*b*	*c*	(wt.%)
VN/Co-NC	VN	*Fm*-3*m*	4.1390(7)	4.1390(7)	4.1390(7)	47
	Co	*Fm*-3*m*	3.5483(6)	3.5483(6)	3.5483(6)	53
VN-NC	VN	*Fm*-3*m*	4.1842(3)	4.1842(3)	4.1842(3)	100
Co-NC	Co	*Fm*-3*m*	3.5425(5)	3.5425(5)	3.5425(5)	100
VN/Co-NC-4	VN	*Fm*-3*m*	4.1446(9)	4.1446(9)	4.1446(9)	71
	Co	*Fm*-3*m*	3.5512(5)	3.5512(5)	3.5512(5)	29
VN/Co-NC-8	VN	*Fm*-3*m*	4.1463(7)	4.1463(7)	4.1463(7)	87
	Co	*Fm*-3*m*	3.5602(6)	3.5602(6)	3.5602(6)	13

Note: phase abundance means the relative phase amount between VN and Co.

Table S3. Structural parameters from nonlinear least-squares fits to the first peak of the Fourier transform at the Co *K*-edge EXAFS of VN/Co-NC and Co-NC.

Samples	Path	*r* (Å)	σ^2 ($\times10^{-3}$ Å^2)	ΔE (eV)	*N*	*R*
VN/Co-NC	Co-Co	2.511 ± 0.011	0.407 ± 0.101	–1.32 ± 1	12 ± 0.1	0.041
Co-NC	Co-Co	2.497 ± 0.013	0.348 ± 0.105	–1.06 ± 1	12 ± 0.1	0.012

Note: *r*: bond length; σ^2: Debye-Waller factor (disorder); ΔE: inner shell potential shift
R: *R*-factor; *N*: coordination number to the Co center

Table S4. The comparison of HER activity of VN/Co-NC with those of recently reported TM-

NC catalysts in alkaline solution.

Material	Electrolyte	η_{10} (mV)	Tafel slope (mV dec^{-1})	Ref.
Co/N,S,Co-G	1.0 M KOH	247	86	S1
Co/CoN/Co_2P-NPC	1.0 M KOH	99	51	S2
Co-NC/GD	1.0 M KOH	284	115	S3
Co@N-CS/N-HCP@CC	1.0 M KOH	66	65	S4
Ni/NC	1.0 M KOH	219	101	S5
Co@BCN	1.0 M KOH	183	73.2	S6
Co@NG-acid	1.0 M KOH	220	112	S7
$Ni_{0.5}Co_{0.5}$/NC	1.0 M KOH	176	132.1	S8
Co-PNCNF	1.0 M KOH	249	92	S9
Co-NCNT/CC	1.0 M KOH	180	193	S10
Mo/Co@NC	1.0 M KOH	157	148	S11
VN-Co/CC*	1.0 M KOH	195	97	S12
Ni@NC	1.0 M KOH	205	160	S23
FeCo@NGC	1.0 M KOH	211	77	S14
Co/NBC	1.0 M KOH	117	146	S15
Co-NC/CNT	1.0 M KOH	203	125	S16
Co@N-CNTs@rGO	1.0 M KOH	108	55	S17
VN/Co-NC	1.0 M KOH	44	51	This work

Table S5. The comparison of HER activity of VN/Co-NC with those of recently reported TM-

NC catalysts in acidic solution.

Material	**Electrolyte**	η_{10} **(mV)**	**Tafel slope (mV dec^{-1})**	**Ref.**
CoNC/GD	0.5 M H_2SO_4	160	207	S3
Co@BCN	0.5 M H_2SO_4	96	63.7	S6
Co@NG	0.5 M H_2SO_4	183	100	S7
Co-NCNT/CC	0.5 M H_2SO_4	78	74	S10
Co-NC/NRGO	0.5 M H_2SO_4	229	126	S18
CoNi@NC	0.5 M H_2SO_4	142	104	S19
Mo/Co@NC	0.5 M H_2SO_4	187	82	S11
Co/N,O-C	0.5 M H_2SO_4	69	46	S20
Co-NRCNT	0.5 M H_2SO_4	260	69	S21
Co/CoN-NC	0.5 M H_2SO_4	190	65	S22
CuCo@NC	0.5 M H_2SO_4	145	79	S23
FeCo@NGC	0.5 M H_2SO_4	262	174	S14
Co-SAC	0.5 M H_2SO_4	260	84	S24
Co@N-CNTs@rGO	0.5 M H_2SO_4	87	52	S17
Co@NC-G-700	0.5 M H_2SO_4	140	62	S25
VN/Co-NC	0.5 M H_2SO_4	22	31	This work

Table S6. Comparison of electrocatalytic HER activity of VN/Co-NC with recently reported transition metal-carbon-based catalysts in acidic media.

Materials	**Electrolyte**	**η@10 mA cm^{-2} (mV)**	**Tafel slope (mV dec^{-1})**	**Durability (Time or Cycle times/Retention)**	**Reference**
MoP/C HCSs	0.5 M H_2SO_4	150	67	24 h/~100%	S26
MoP/NPG	0.5 M H_2SO_4	148	49	60 h/~61%	S27
WS_2@Graphene	0.5 M H_2SO_4	117	56	10000 cycles/~75%	S28
Fe_2N/C	0.5 M H_2SO_4	110	41.2	50 h/~100%	S29
V-MoS_2/VG	0.5 M H_2SO_4	98	49	32 h/~95%	S30
Co_9S_8/MoS_2/C	0.5 M H_2SO_4	97	71	10 h/~95%	S31
Co@N-CNTs@rGO	0.5 M H_2SO_4	87	52	100 h/~100%	S17
Ru-RuO_2/CNT	0.5 M H_2SO_4	63	31	1500 cycles/~75%	S32
CoP/NiCoP/NC	0.5 M H_2SO_4	60	58	80 h/~67%	S33
FeP/C	0.5 M H_2SO_4	51.1	41.7	40 h/~100%	S34
VN-Co/NC	0.5 M H_2SO_4	22	31.0	72 h/~100%	This work

Table S7. Comparison of electrocatalytic HER activity of VN/Co-NC with recently reported transition metal-carbon-based catalysts in alkaline media.

Materials	**Electrolyte**	**η@10 mA cm^{-2} (mV)**	**Tafel slope (mV dec^{-1})**	**Durability (Time or Cycle times/Retention)**	**Reference**
Mo_2C/CF	1.0 M KOH	161	82	10 h/~80%	S35
CoP@NPCP	1.0 M KOH	150	20	15 h/~75%	S36
MoP/NPG	1.0 M KOH	126	56	12 h/~61%	S27
MoC-Mo_2C/PNCDs	1.0 M KOH	121	60	20 h/~58%	S37
$Mo_{1.33}W_{0.67}C$@NC	1.0 M KOH	108	55.4	20 h/~90%	S38
Co@N-CNTs@rGO	1.0 M KOH	108	55	100 h/~98%	S17
WC-W_2C/PNCDs	1.0 M KOH	101	90	20 h/~58%	S37
MoP@NCHs	1.0 M KOH	92	62	40000 s/~100%	S39
CoP_2@NPC	1.0 M KOH	90	54	10 h/~90%	S40
CoP/NiCoP/NC	1.0 M KOH	75	64	3000 cycles/~67%	S33
VN-Co/NC	1.0 M KOH	44	51.0	72 h/~100%	This work

Table S8. Comparison of electrocatalytic HER activity of VN/Co-NC with recently reported transition metal-carbon-based catalysts in neutral media.

Materials	**Electrolyte**	**η@10 mA cm^{-2} (mV)**	**Tafel slope (mV dec^{-1})**	**Durability (Time and cycles)**	**Reference**
Mo_2C@N-CANs	0.1 M PBS	350	94.7	24 h/~83%	S41
NiSe@NC	1.0 M PBS	300	66.2	12 h/~100%	S42
P-Fe_3O_4@3DG	1.0 M PBS	295.4	234.6	50 h/~100%	S43
Co_9S_8/NC@MoS_2	1.0 M PBS	261	126.1	12 h/~50%	S44
Mo-WC@NCS	1.0 M PBS	221	95	12 h/~80%	S45
MoP NA/CC	1.0 M PBS	187	94	46 h/~100%	S46
$Ni_{0.85}$Se@NC	1.0 M PBS	183	-	10 h/99.1%	S47
Ni/*β*-Mo_2C@PC	1.0 M PBS	179	106	24 h/~99%	S48
MoS_2@CoO/CC	1.0 M PBS	176	-	10 h/~67%	S49
CoP/C	1.0 M PBS	161	81	70000 s/~67%	S50
VN-Co/NC	1.0 M PBS	163	117	72h/~100%	This work

Table S9. Comparison of electrocatalytic HER activity of VN/Co-NC with recently reported carbon free transition metal-based catalysts in neutral media.

Materials	Electrolyte	η@10 mA cm^{-2} (mV)	Tafel slope (mV dec^{-1})	Durability (Time/Retention)	Reference
CoFeO@BP	1.0 M KOH	88	51	24 h/~90%	S51
$Ni_{17}W_3$–W hybrid	1.0 M KOH	59	52	24 h/~90%	S52
$Ni_2P/NiTe_2$	1.0 M KOH	62	80	20 h /~80%	S53
Ni_3Se_4/Ni_3S_2/NF	1.0 M KOH	89	61	11 h/~99%	S54
O-CoP	1.0 M KOH	116	59	19 h/~80%	S55
1T-MoS_2/CoS_2	1.0 M KOH	71	60	72 h/~90%	S56
Ni_5P_4	1.0 M NaOH	49	98	16 h/—	S57
3D-NiCoP	1.0 M KOH	105	79	16 h/~90%	S58
FeP/Ti	1.0 M KOH	95	—	10 h/~50%	S59
VN-Co/NC	1.0 M KOH	44	51.0	72 h/~100%	This work
Ni_5P_4	1.0 M H_2SO_4	23	33	16 h/—	S57
3D-NiCoP	0.5 M H_2SO_4	80	37	16 h/~99%	S58
FeP/Ti	0.5 M H_2SO_4	79	—	10 h/~88%	S59
$Co_{0.97}Ti_{0.03}SP$	0.5 M H_2SO_4	44	51	12 h/~91%	S60
$RuRh_2$	0.5 M H_2SO_4	34	17	30000 cycles /~99%	S61
$Cr_{0.4}Mo_{0.6}B_2$	0.5 M H_2SO_4	193	60.1	25 h/~93%	S62
MoO_2/MoS_2|P	0.5 M H_2SO_4	85	49.7	2000 cycles /~95%	S63
FeP/Ti	0.5 M H_2SO_4	50	—	16 h/~71%	S64
Ni_2P	0.5 M H_2SO_4	~120	46	500 cycles/—	S65
Co_2P/Ti	0.5 M H_2SO_4	95	45	24 h/—	S66
Ni_2P	0.5 M H_2SO_4	~160	75	500 cycles/—	S67
VN-Co/NC	0.5 M H_2SO_4	22	31.0	72 h/~100%	This work
FeP/Ti	1.0 M PBS	102	—	16 h/~83%	S64
Ni_3Se_4/Ni foam	1.0 M PBS	160	—	1000 cycles /~100%	S68
RhCu	1.0 M PBS	57	95	12 h/~99%	S69

nanotubes					
NiCu-P	1.0 M PBS	250	96	1000 cycles	S70
MoS_2@CoO	1.0 M PBS	176	—	10 h/—	S71
Ni−Co−S film	1.0 M PBS	280	93	6.5 h/~82%	S72
CoO/Co_4N/NF	1.0 M PBS	145	80	50 h/~80%	S73
$NiFe_2O_4$/NF	1.0 M PBS	197	81.3	—/—	S74
MoP700	1.0 M PBS	196	79	2 h/~86%	S75
VN-Co/NC	1.0 M PBS	163	117	72 h/~100%	This work

Table S10. Comparison of stability of Co-amount after HER cycling for Co-NC electrocatalysts prepared by one-pot treatment and multiple-step treatment.

Co-NC	**Total amount of catalyst for cycling**	**Co-amount in catalyst**	**Co-amount in electrolyte after 1000 LSV cycles**	**Dissolution ratio of Co**
One-pot	0.06 mg	72 wt.%	0.0028 mg	6.5%
Multiple-step	0.06 mg	45 wt.%	0.0019 mg	7.0%

Table S11. Comparison of TOF values of VN/Co-NC with Co-NC, V-NC, NC and Pt@C in 0.5 M H_2SO_4, 1.0 M KOH and 1.0 M PBS solution, respectively.

Catalysts	Electrolytes	C_{dl}	ECSA (cm^2)	Constant in formula	TOF@100 mV
VN-Co/NC	0.5 M H_2SO_4	36.6	915	0.0740	7.07
	1.0 M KOH	38.6	965	0.0701	4.9
	1.0 M PBS	27.0	675	0.1003	0.24
Co/NC	0.5 M H_2SO_4	28.8	720	0.0940	0.19
	1.0 M KOH	30.6	765	0.0885	0.13
	1.0 M PBS	22.9	572.5	0.1182	0.05
VN/NC	0.5 M H2SO4	21	525	0.1289	0.02
	1.0 M KOH	11.2	280	0.2417	0.03
	1.0 M PBS	49.4	1235	0.0548	0.13
NC	0.5 M H_2SO_4	16.9	422.5	0.1602	0.018
	1.0 M KOH	9.8	245	0.2762	0.094
	1.0 M PBS	24.2	605	0.1119	0.048
Pt@C	0.5 M H_2SO_4	35.3	882.5	0.0022	0.127
	1.0 M KOH	23.3	582.5	0.0033	0.113
	1.0 M PBS	46.8	1170	0.0016	0.102

Table S12. Comparison of TOF values of VN/Co-NC with recently reported metal-based catalysts.

Materials	Electrolyte	Overpotential (mV)	TOF (s^{-1})	References
Ni_5P_4	0.5 M H_2SO_4	100	3.5	S57
Ni_2P	0.5 M H_2SO_4	100	0.015	S65
Co_2P	0.5 M H_2SO_4	100	0.272	S76
CC@N-CoP	0.5 M H_2SO_4	50	0.0199	S77
np-$(Co_{0.52}Fe_{0.48})_2P$	0.5 M H_2SO_4	50	0.1	S78
WC nanocrystalline	0.5 M H_2SO_4	181	1	S79
WC nanowall	0.5 M H_2SO_4	126	1	S79
MoP@NC	0.5 M H_2SO_4	100	0.28	S80
WP@NC	0.5 M H_2SO_4	100	0.05	S80
MoP	0.5 M H_2SO_4	100	0.024	S81
W/BrN	0.5 M H_2SO_4	200	1	S82
MoS_2	0.5 M H_2SO_4	200	0.29	S83
P-Fe_3O_4@3DG	0.5 M H_2SO_4	100	0.0048	S43
Nv-Fe_2N/C	0.5 M H_2SO_4	100	0.064	S29
PtRu@RFCS	0.5 M H_2SO_4	100	4.03	S84
Co-NG	0.5 M H_2SO_4	100	0.101	S85
VN-Co/NC	0.5 M H_2SO_4	100	7.07	This work
Ni_5P_4	1.0 M KOH	100	0.79	S57
Pt/C	1.0 M KOH	50	0.27	S86
Au-Ru	1.0 M KOH	50	0.31	S86

3.0% S-CoO NRs	1.0 M KOH	100	0.41	S87
Ni-doped MoS_2	1.0 M KOH	100	0.08	S88
Ni_5P_4 catalysts	1.0 M KOH	100	0.05	S89
Ru@C_2N	1.0 M KOH	25	0.67	S90
P-Fe_3O_4@3DG	1.0 M KOH	100	0.0017	S83
Ni-P/Ni/NF	1.0 M KOH	230	5.36	S91
P-MoP/Mo_2N	1.0 M KOH	100	0.06	S92
$NiMoO_x$/NiMoS	1.0 M KOH	100	1.97	S93
$PtSn_4$	1.0 M KOH	100	1.54	S86
VN-Co/NC	1.0 M KOH	100	4.9	This work
NiCoN|Ni_xP|NiCoN	1.0 M PBS	300	0.771	S94
P-MoP/Mo_2N	1.0 M PBS	100	0.049	S92
$NiCo_2Te_4$	1.0 M PBS	100	6.5	S95
Ni/$Ni(OH)_2$	1.0 M PBS	110	4.99	S96
CoS_2@MoS_2/CP	1.0 M PBS	200	4.2	S97
$CoMoS_4$ NS/CC	1.0 M PBS	200	0.2	S98
Pt/np-$Co_{0.85}Se$	1.0 M PBS	100	3.93	S99
VN-Co/NC	1.0 M PBS	100	0.24	This work

S1 Estimation for the TOF

Take calculating TOF of VN-Co/NC in acidic media as an example. According to literature procedures, the following steps were performed to calculate TOFs. First, electrochemically active surface area (ECSA) was calculated as below.

$$A_{ECSA} = \frac{The\ capacitance\ of\ the\ double\ layer\ C_{dl}}{The\ specific\ capacitance\ of\ per\ real\ surface\ area}$$

In general, the specific capacitance for a flat surface is found to be in the range of 20-60 μF/cm^2.We adopt the medium value of 40 μF/cm^2 to calculate the turnover frequency (TOF) of heterostructures of VN and Co embedded in N-doped carbon electrocatalysts (VN-Co/NC). In 0.5 M H_2SO_4, the measured C_{dl} of VN-Co/NC is 36.6 mF cm^{-2}, so the ECSA of VN-Co/NC was calculated as 915 cm^2.

$$A_{ECSA(VN-Co/NC)} = \frac{36.6\ mF\ cm^{-2}}{40\ \mu F\ cm^{-2}} = 915\ cm^2$$

For HER, TOF refers to the number of H_2 turnover per active site, which could be calculated using the following formula.

$$TOF = \frac{number\ of\ total\ H_2\ turnover/geometric\ area}{number\ of\ active\ sites/geometric\ area}$$

With a ~100% Faraday efficiency, the number of total H_2 turnover (n_{H2}) at different current density (j) can be calculated as follows.

$$n_{H2} = \left(j\frac{mA}{cm^2}\right)\left(\frac{1\ Cs^{-1}}{1000\ mA}\right)\left(\frac{1\ mol\ e^-}{96485.3\ C}\right)\left(\frac{1\ mol\ H_2}{2\ mol\ e^-}\right)\left(\frac{6.022\times10^{23}\ H_2}{1\ mol\ H_2}\right)$$

$$n_{H2} = 3.12\times10^{15}\frac{H_2/s}{cm^2}per\frac{mA}{cm^2}$$

In this work, the poison tests and *in-situ* Raman spectra confirmed the active site of VN-Co/NC should be carbon. In graphite, the hexagonal layered structure with bond lengths of 1.42 Å for six-membered ring and layer spacing of 3.40 Å shows a volume of 17.8 Å^3. Moreover, it is noted that each C atom is shared by 6 cells, thus the number of C atoms per unit cell is regarded as 2. Thus, the area density of carbon atoms ($n_{carbon\ atoms}$) could be calculated.

$$n_{carbon\ atoms} = \left(\frac{2\ atoms\ per\ unit\ cell}{17.8\ Å^3\ per\ unit\ cell}\right)^{2/3} = 2.33\times10^{15} atoms\ per\ cm^2$$

Since the real active site is the carbon atom near to the N atom, the exact number of "active" carbon sites could then be calculated according to the dopant's concentration[S100] and active species in dopant as:

$$n_{active\ sites} = n_{carbon\ atoms}\times concentration\ of\ N$$

$$n_{active\ sites} = 2.33\times10^{15}\times1.98\% = 4.61\times10^{13}\ atoms\ per\ cm^2$$

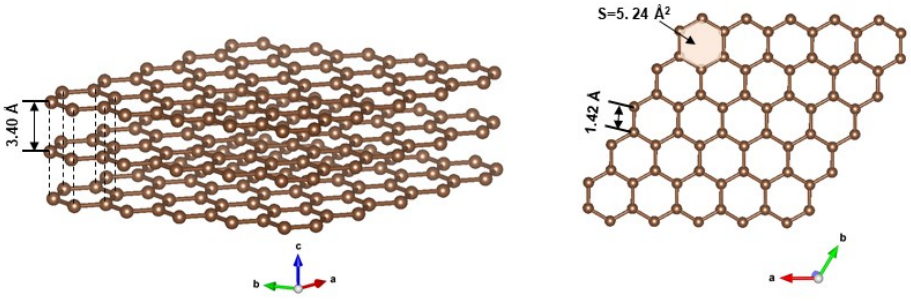

Crystal structure and cell parameters of 3D graphite.

Therefore, the LSV curve of VN-Co/NC was converted to a curve of TOF and potential according to the following calculation.

$$TOF_{VN-CO/NC} = \frac{\left(3.12 \times 10^{15} \frac{H_2/s}{cm^2} per \frac{mA}{cm^2}\right) \times |j|}{n_{active\ sites} \times A_{ECSA}}$$

$$TOF_{VN-CO/NC} = \frac{\left(3.12 \times 10^{15} \frac{H_2/s}{cm^2} per \frac{mA}{cm^2}\right) \times |j|}{(4.61 \times 10^{13} atoms\ per\ cm^2) \times 915\ cm^2} = 0.0740 \times |j|$$

For reference samples (i.e., VN-NC, Co-NC and NC), carbon atoms near to the N were also assumed as active sites to calculate corresponding TOFs. Eventually, in 0.5 M H_2SO_4, the current densities of VN-NC, Co-NC and NC were converted into TOF plots as below.

$TOF_{CO/NC} = 0.0940 \times |j|$

$TOF_{VN/NC} = 0.129 \times |j|$

$TOF_{NC} = 0.160 \times |j|$

As comparison, the ECSA of Pt@C in 0.5 M H_2SO_4 was measured to be 888 cm^2 using double layer capacitance. For Pt@C, 4-surface Pt atoms in unit cell with a volume of 60 $Å^3$ are regarded as active sites, so the area density of active sites was calculated as $1.644 \times 10^{15}\ atoms\ per\ cm^2$. Furthermore, we could use the following equation to calculate the TOF of Pt@C:

$TOF_{Pt@C} = 0.0021 \times |j|$

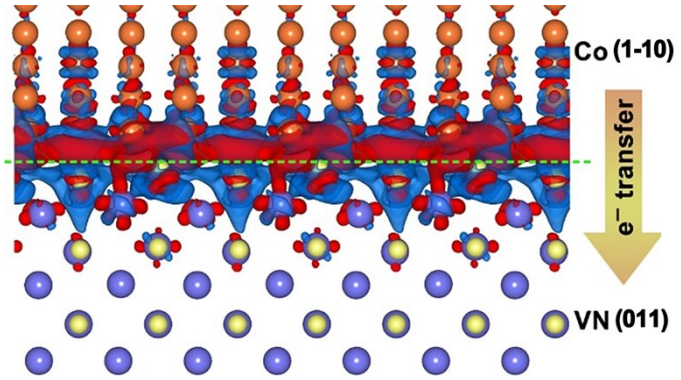

Fig. S1 Charge density redistribution of the heterostructure constructed by joining N-terminated (011) slab of VN and Co-terminated (1-10) slab of Co, showing 22 atoms under the interface, resulting in 0.92 e- transfer from Co to VN.

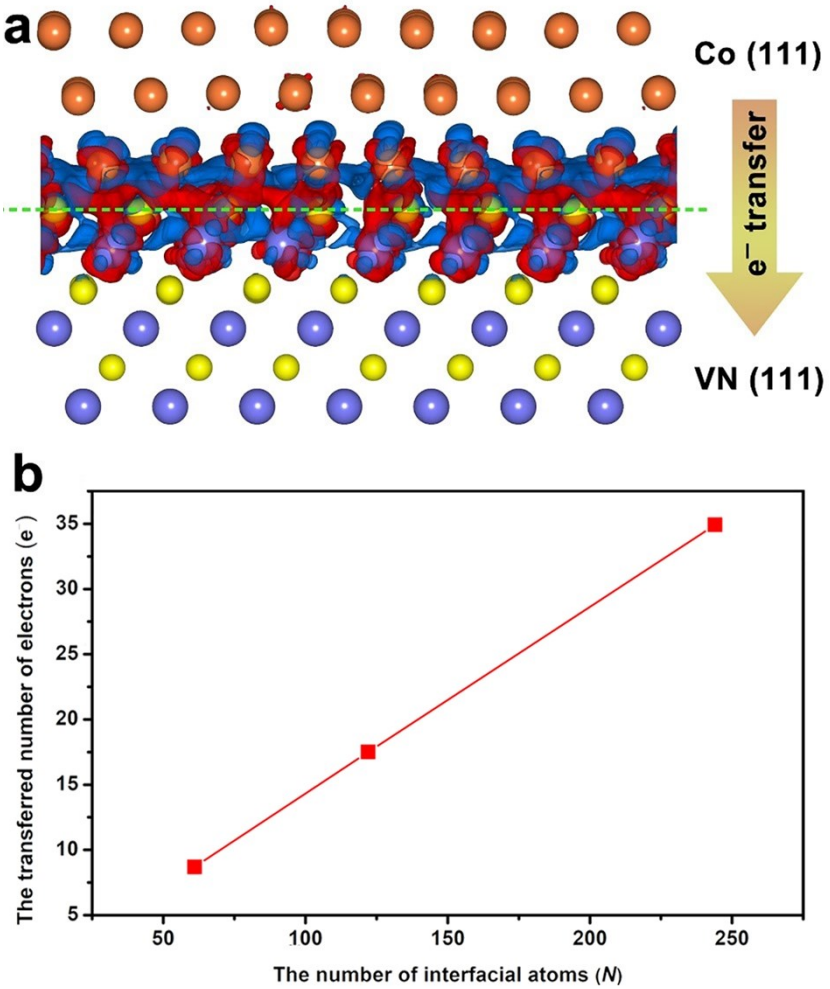

Fig. S2 (a) Charge density redistribution of the heterostructure constructed by joining N-terminated (111) slab of VN and Co-terminated (111) slab of Co, showing 61 atoms under the interface, resulting in 8.7 e^- transfer from Co to VN; (b) the correlation of transferred electron number from Co to VN with the number of interfacial atoms.

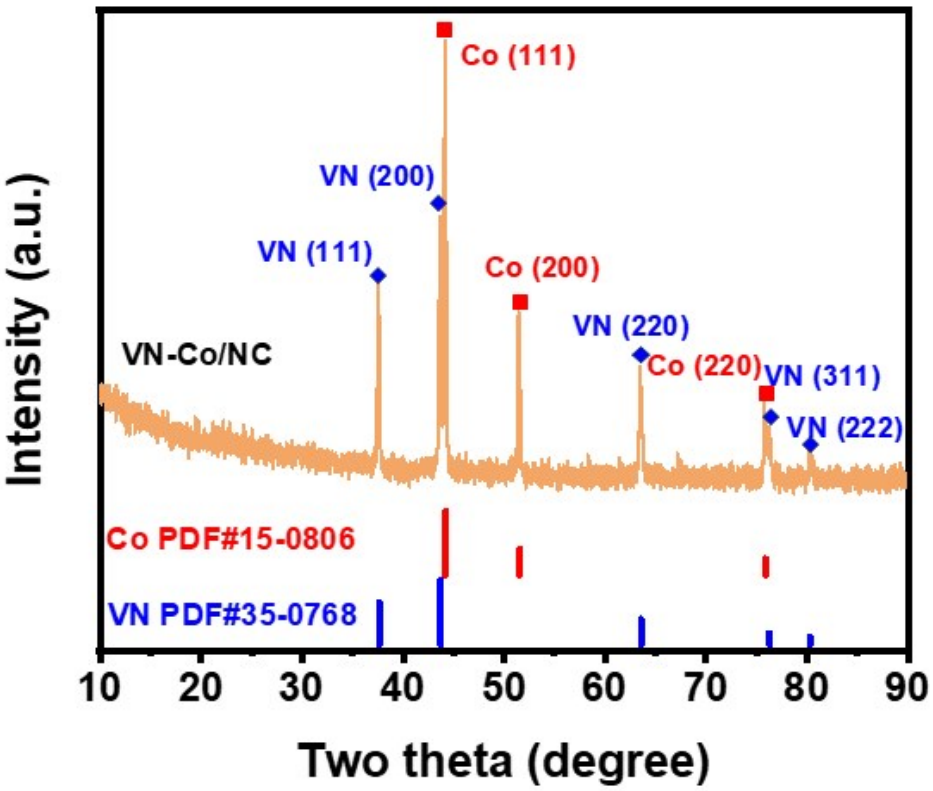

Fig. S3 XRD pattern or VN-Co/NC with the insertion of PDF card and corresponding crystal facets.

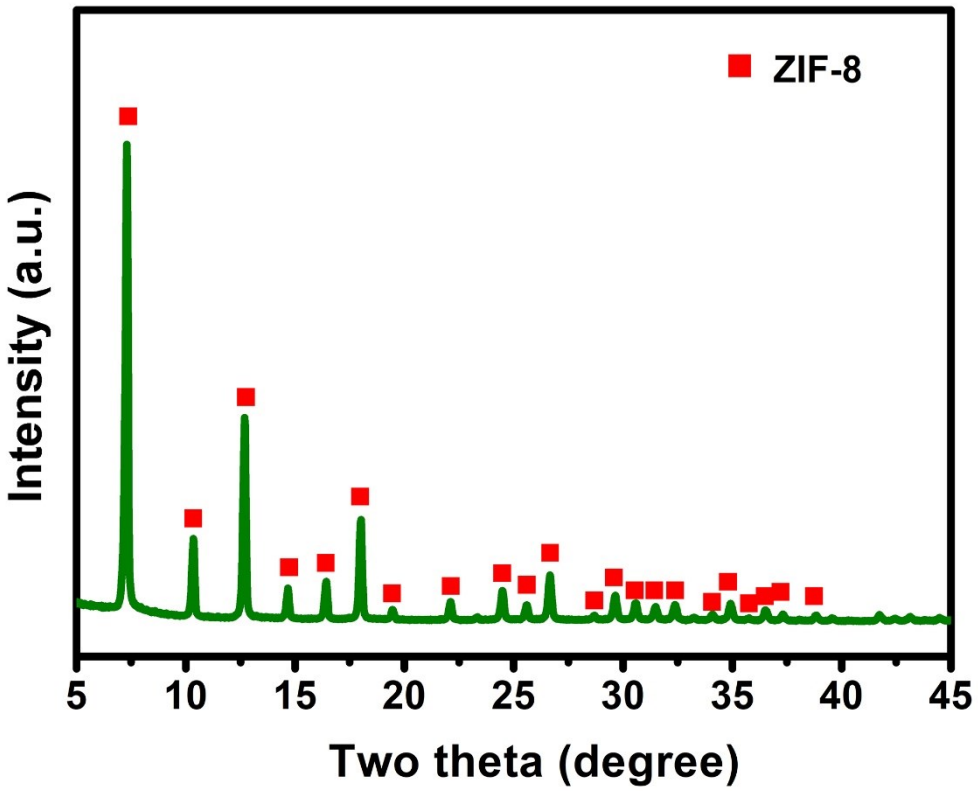

Fig. S4 XRD pattern of as-prepared ZIF-8 precursor.

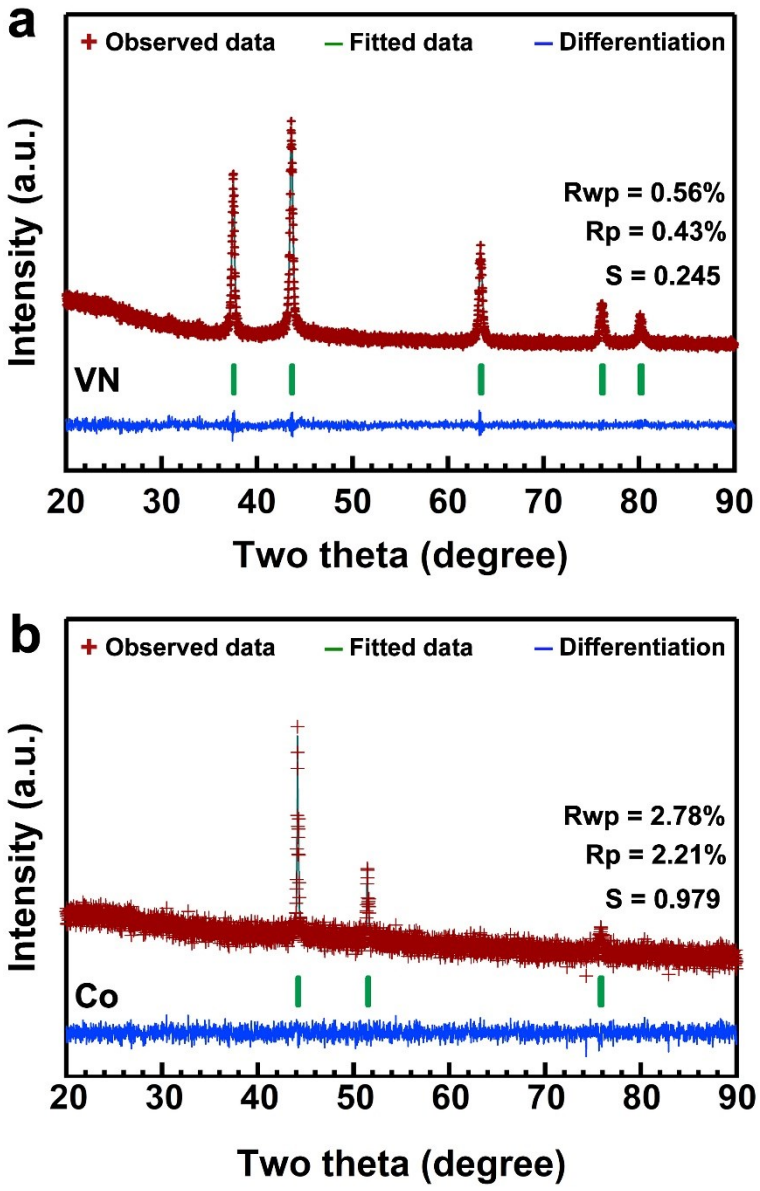

Fig. S5 Rietveld refinement of XRD patterns for (a) VN-NC and (b) Co-NC composites.

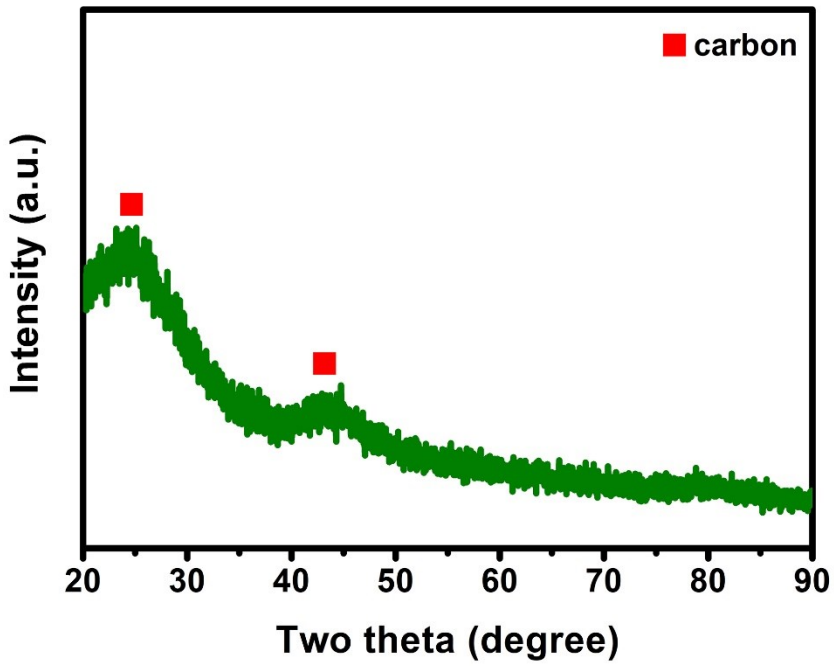

Fig. S6 XRD pattern for the pyrolyzed ZIF-8 precursor under 960 ºC.

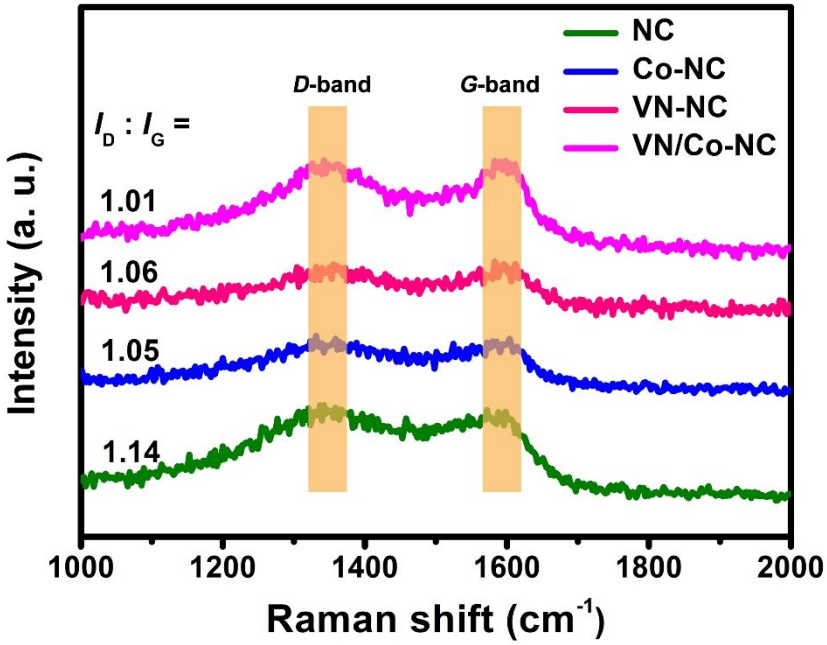

Fig. S7 Raman spectra of VN/Co-NC, VN-NC, Co-NC and NC composites.

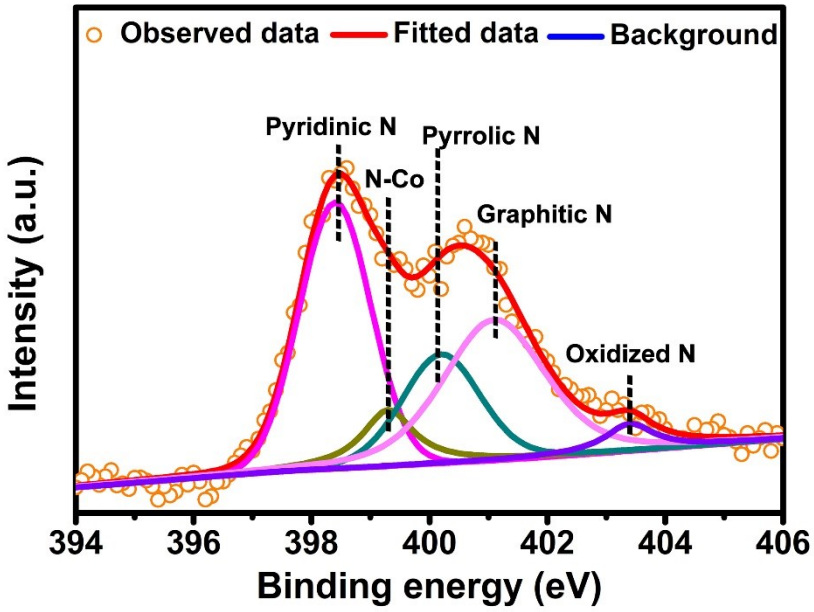

Fig. S8 High-resolution N 1*s* XPS spectra of Co-NC composite.

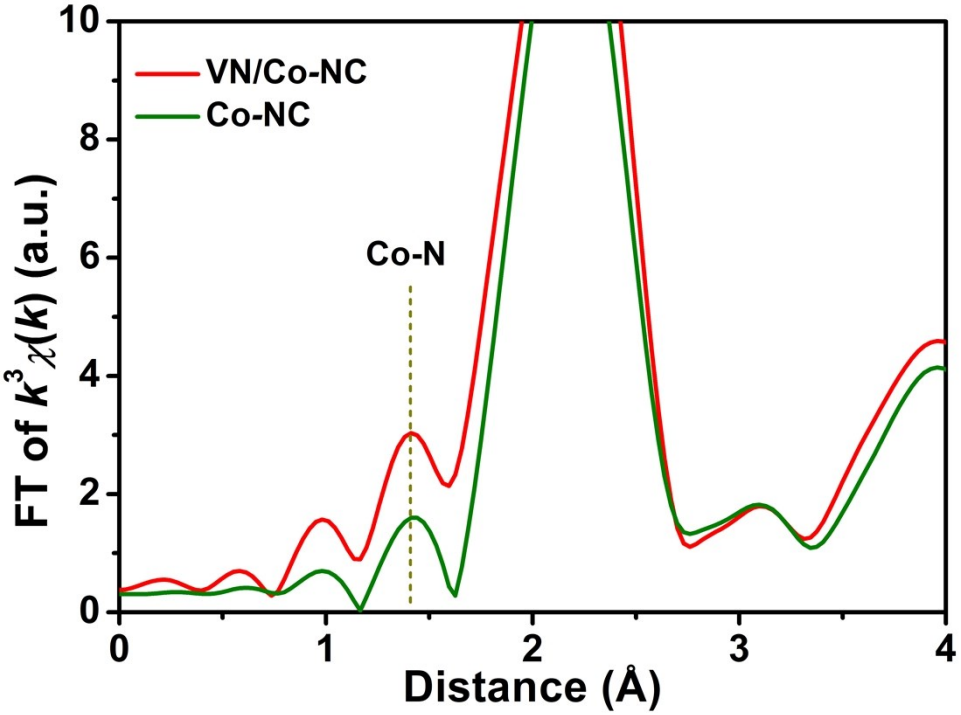

Fig. S9 Comparison of signal showed in EXAFS region corresponding to Co-N bond between VN/Co-NC and Co-NC.

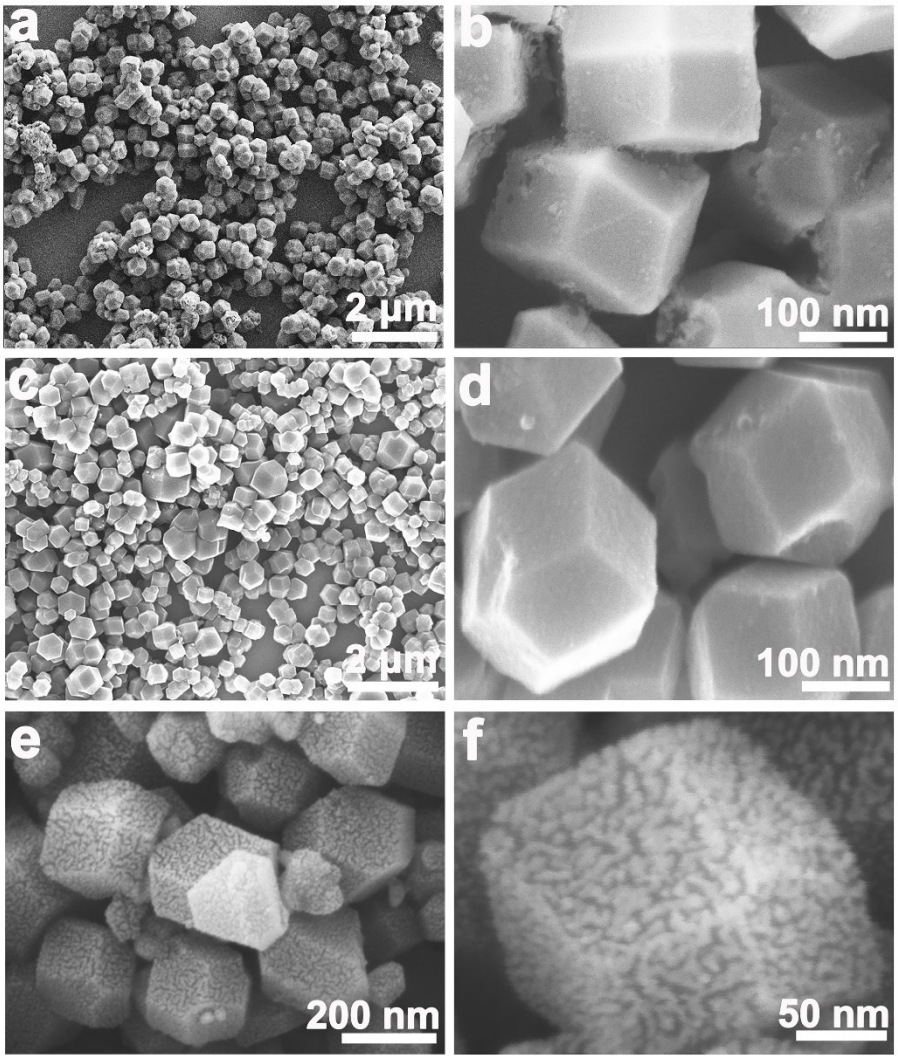

Fig. S10 FESEM images of (a, b) ZIF-8, (c, d) NC, and (e, f) VN/Co-NC composites.

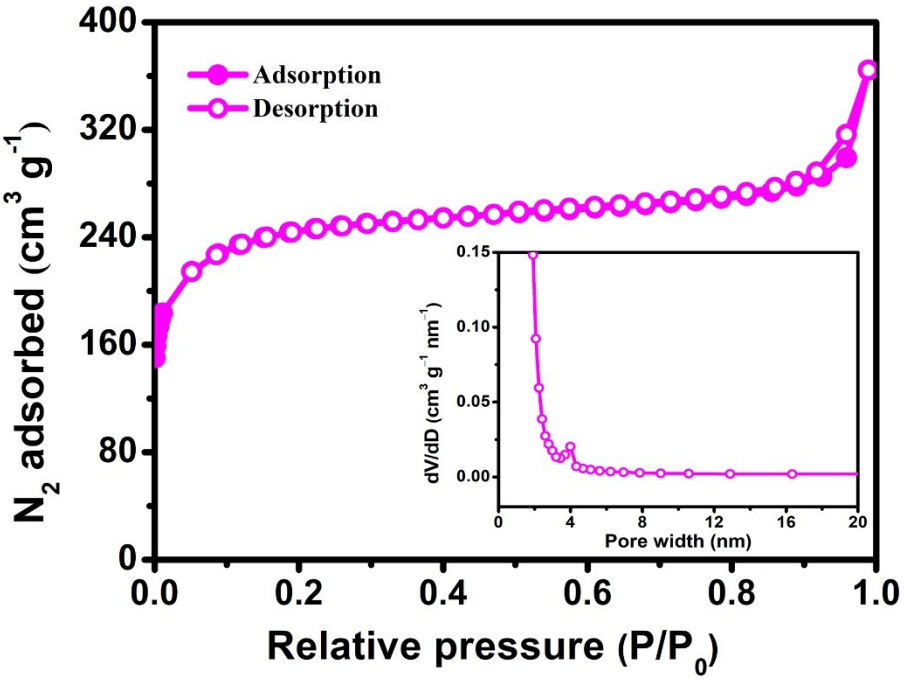

Fig. S11 N_2 ad-/desorption isotherm curves of VN/Co-NC composite under 77 K. The inset: the pore size distribution of VN/Co-NC composite.

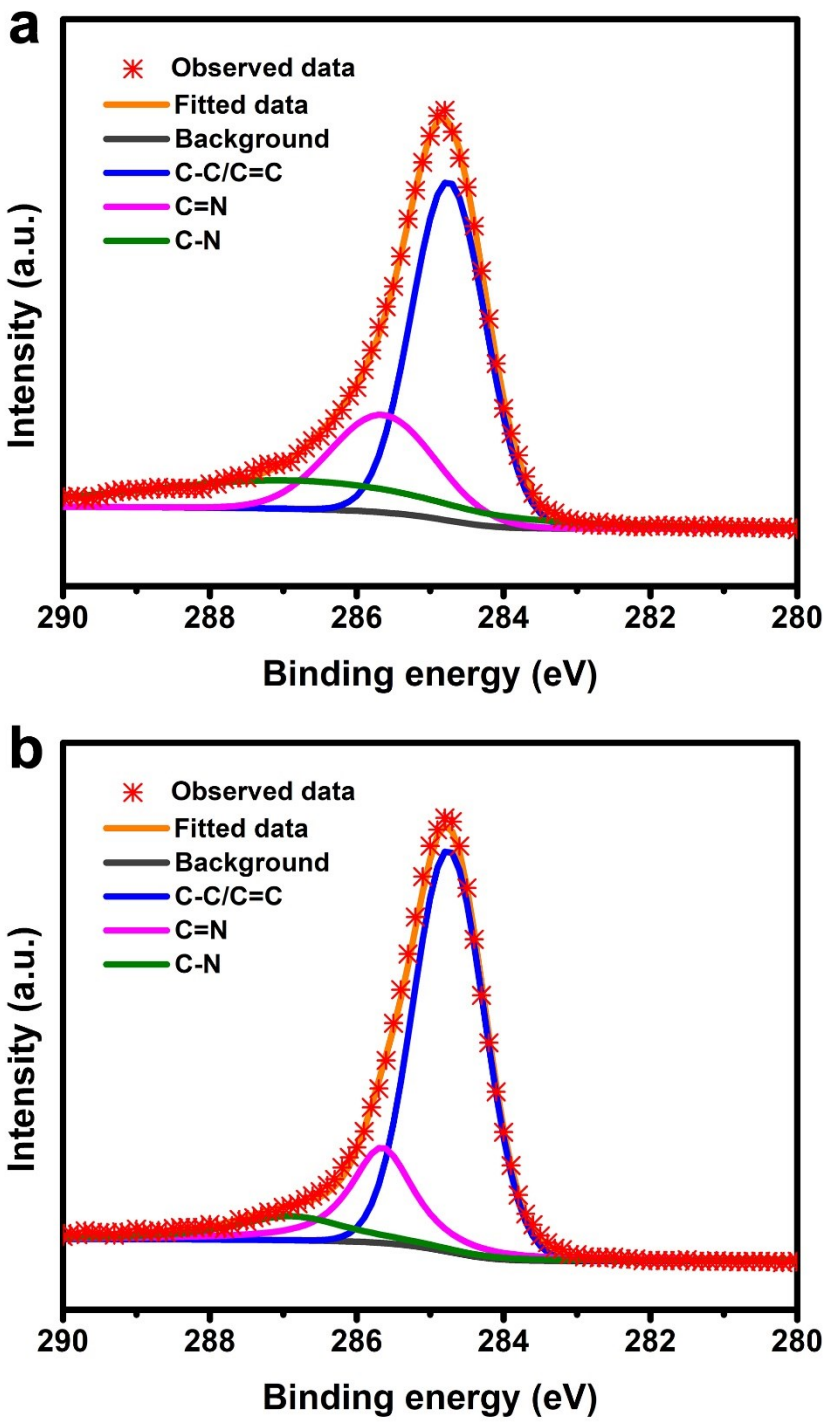

Fig. S12 High-resolution C 1s spectra of (a) NC and (b) VN/Co-NC composites.

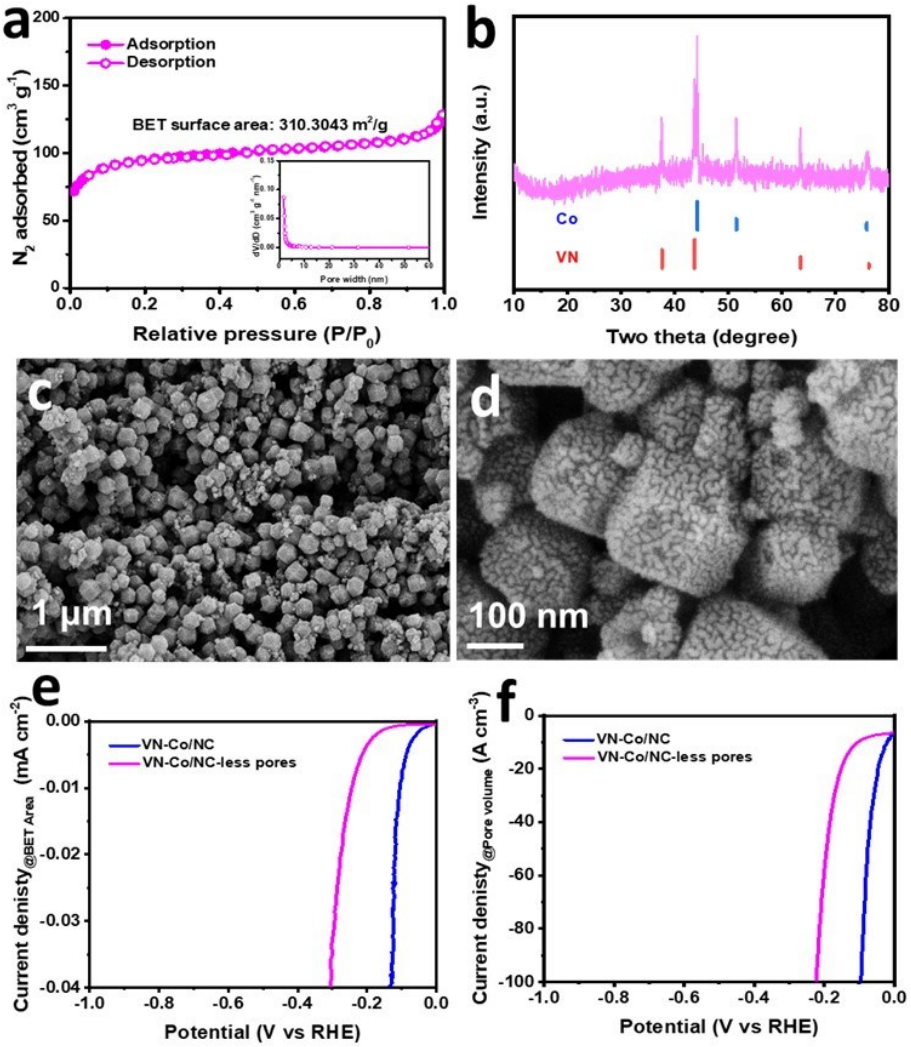

Fig. S13 VN/Co-NC composite with larger particle size: (a) N_2 ad-/desorption isotherm curves under 77 K (the inset: the pore size distribution); (b) XRD pattern; (c) and (d) SEM images; (e) BET surface area normalized LSV curves and (f) pore volume normalized LSV curves.

The VN/Co-NC with larger particle size shows BET surface area of 310 $m^2\ g^{-1}$ and pore volume 0.19 $cm^3\ g^{-1}$. In this experiment, the mass loading of catalyst on GC electrode (~0.8 mg cm^{-2}), BET surface areas and pore volumes of catalyst are used for normalizing the LSV curves.

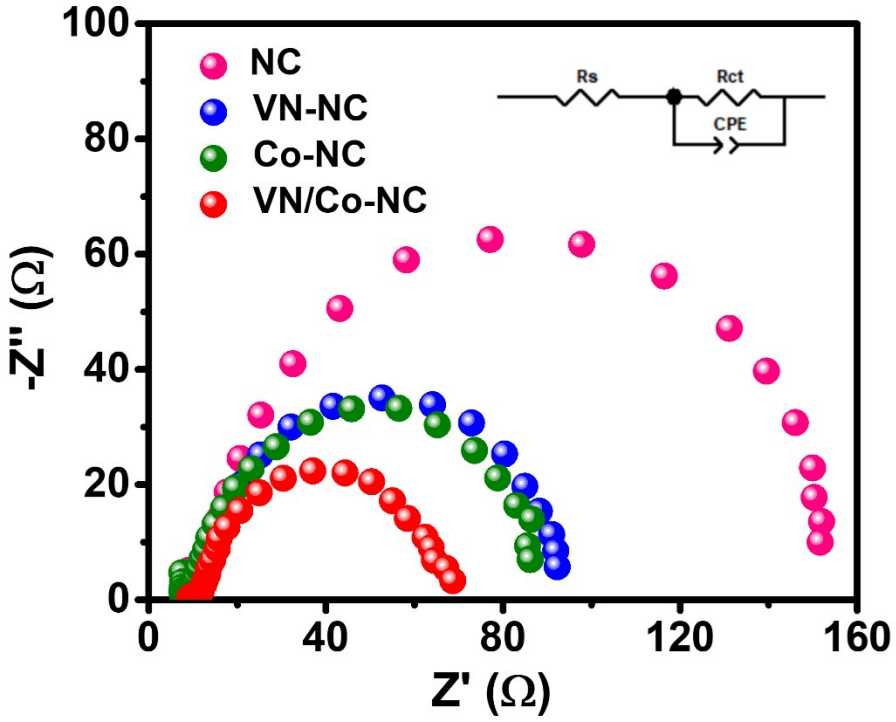

Fig. S14 EIS spectra of VN/Co-NC, Co-NC, VN-NC, and NC composites in 1.0 M KOH solution. The inset: the equivalent circuit modeled from the EIS spectra.

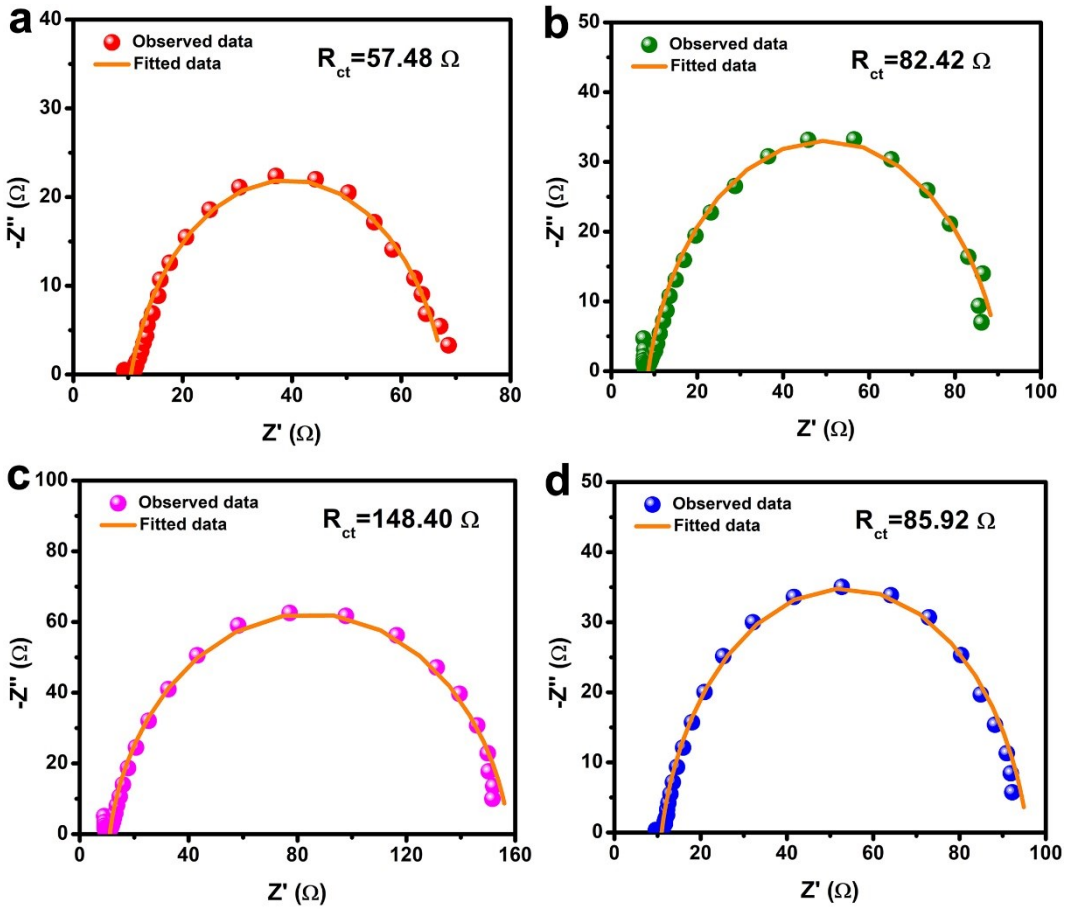

Fig. S15 Fitted results for EIS spectra of VN/Co-NC, Co-NC, NC, and VN-NC composites in 1.0 M KOH solution.

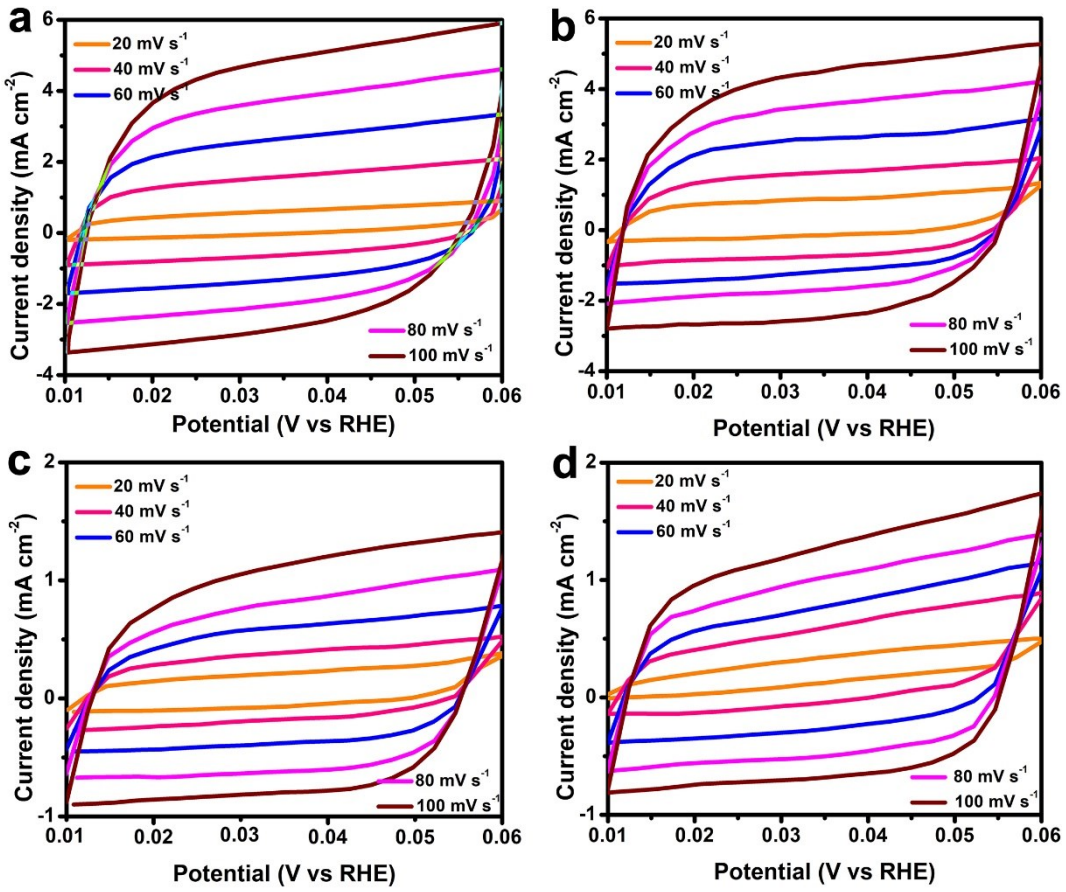

Fig. S16 CV curves at scan rates from 20, 40, 60, 80, to 100 mV s^{-1} for (a) VN/Co-NC, (b) Co-NC, (c) VN-NC, and (d) NC composites within potential ranges from 0.01 to 0.06 V.

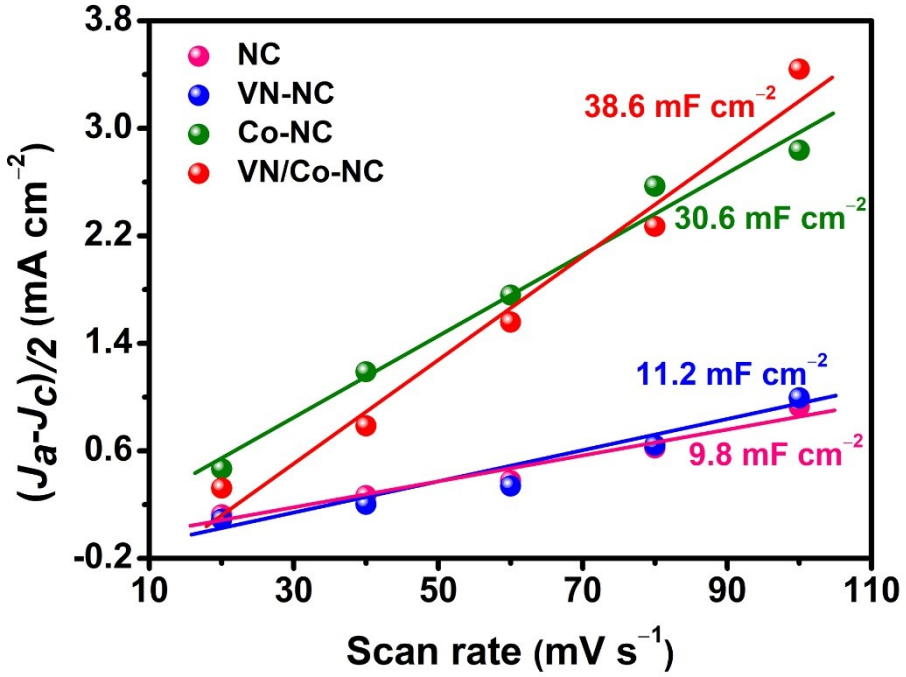

Fig. S17 C_{dl} values for VN/Co-NC, Co-NC, VN-NC, and NC composites in 1.0 M KOH electrolyte.

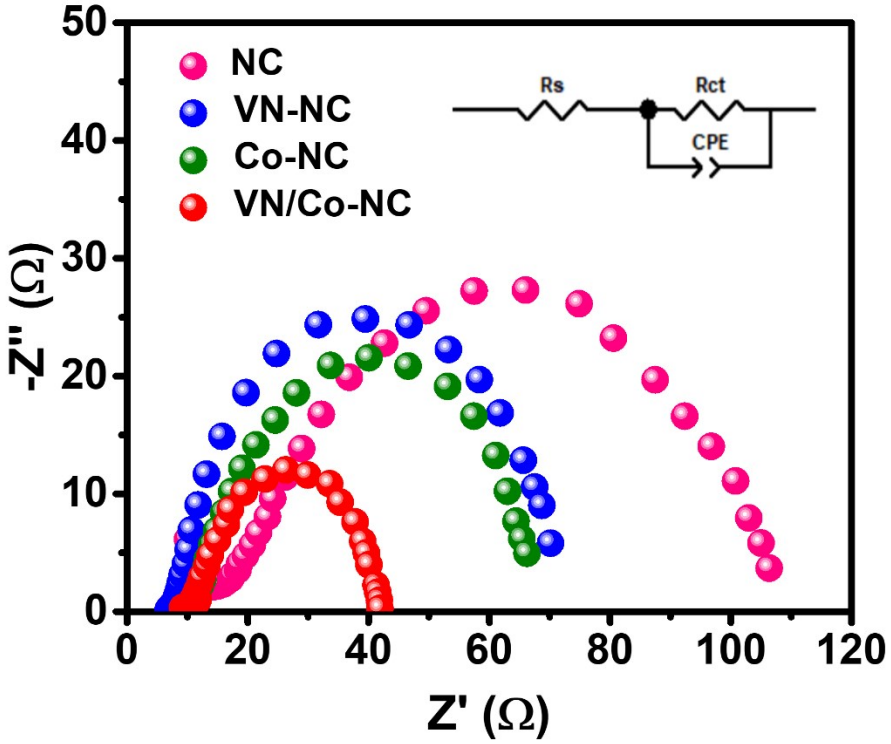

Fig. S18 EIS spectra of VN/Co-NC, Co-NC, VN-NC, and NC composites in 0.5 M H_2SO_4 electrolyte. The inset: the equivalent circuit modeled from the EIS spectra.

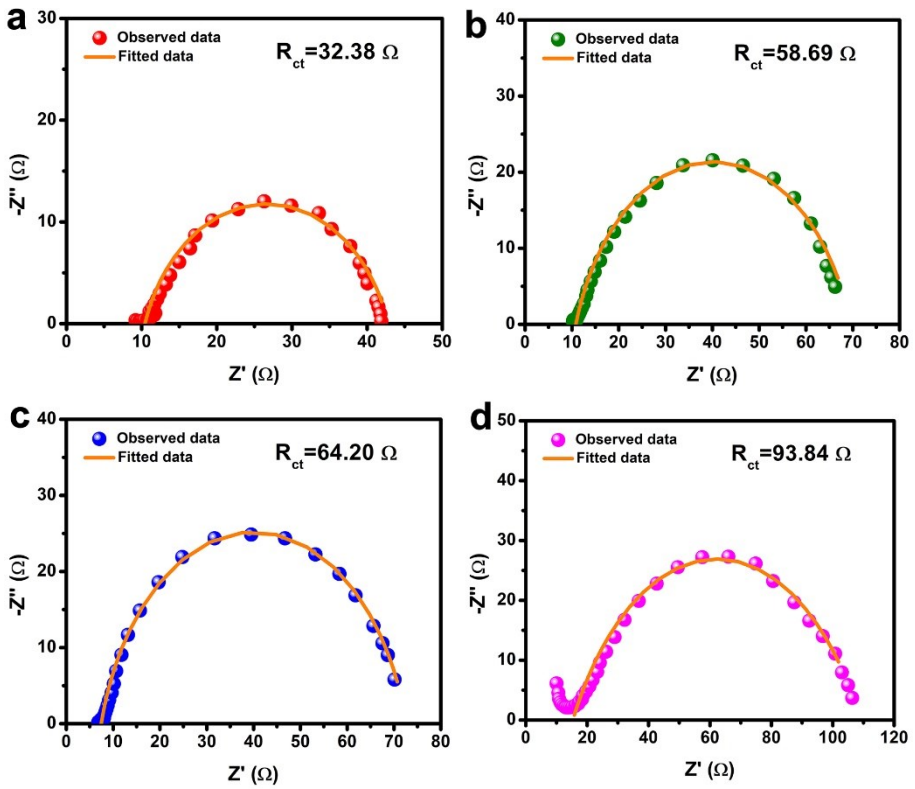

Fig. S19 Fitted results for EIS spectra of VN/Co-NC, Co-NC, VN-NC, and NC composites in 0.5 M H_2SO_4 electrolyte.

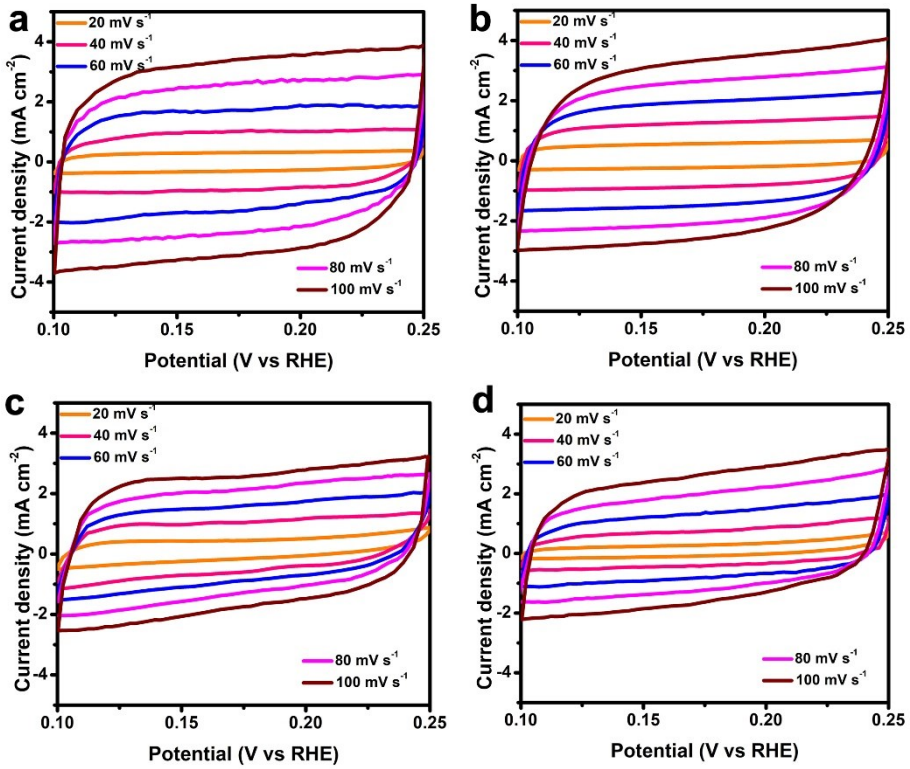

Fig. S20 CV curves at scan rates from 20, 40, 60, 80, to 100 mV s^{-1} for (a) VN/Co-NC, (b) Co-NC, (c) VN-NC, and (d) NC composites within potential ranges from 0.10 to 0.25 V.

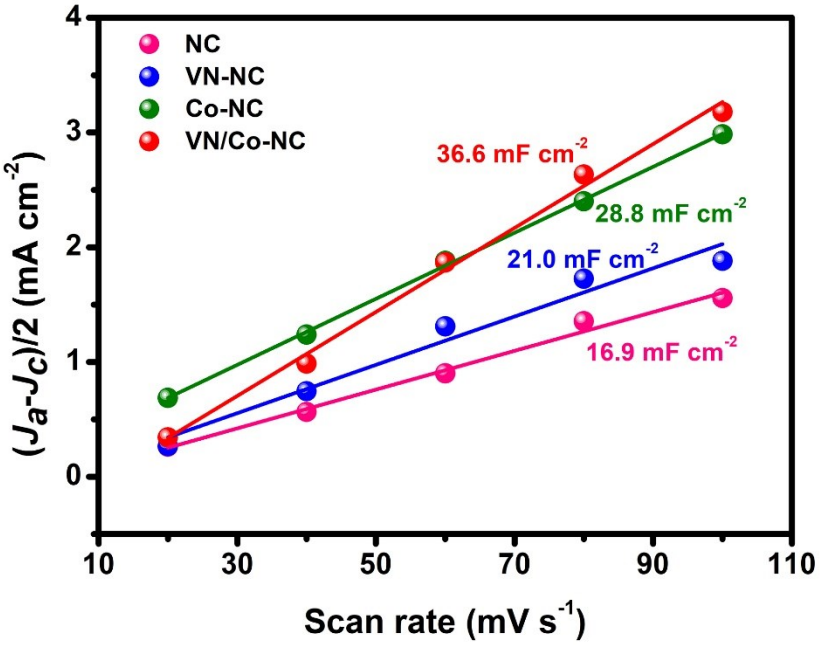

Fig. S21 C_{dl} values for VN/Co-NC, Co-NC, VN-NC, and NC composites in 0.5 M H_2SO_4 electrolyte.

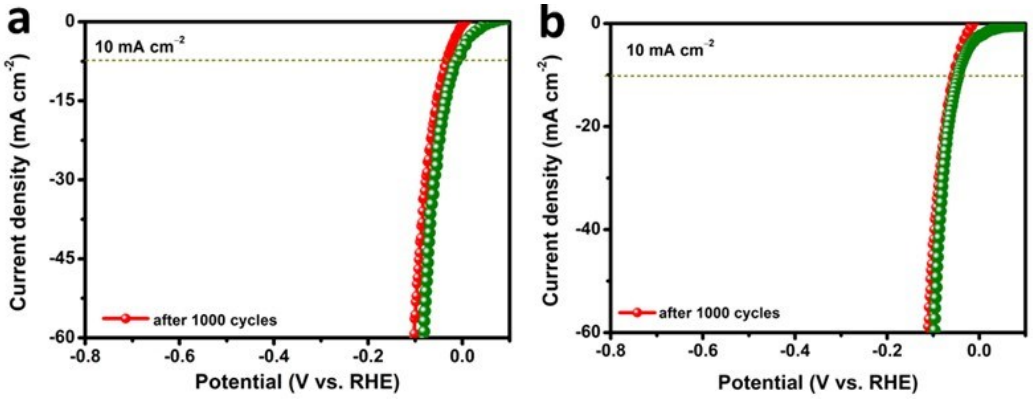

Fig. S22 Comparison of LSV curves of VN/Co-NC composite before and after 1000 cycles in (a) 0.5 M H_2SO_4 and (b) 1.0 M KOH electrolyte.

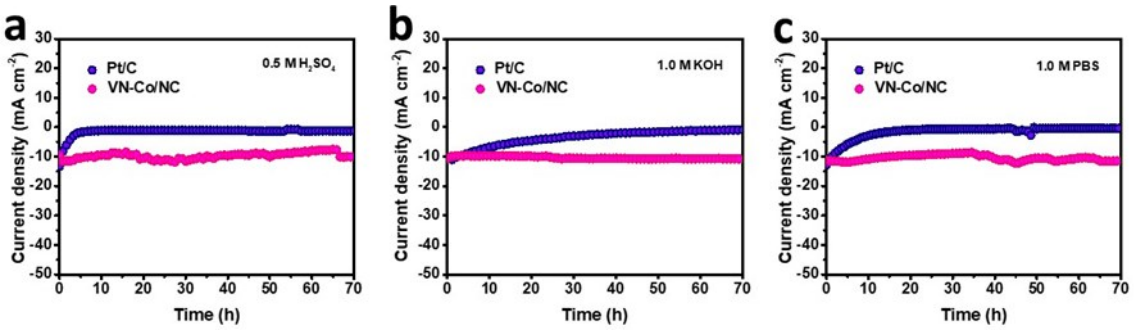

Fig. S23 Comparison of cycling performance of VN/Co-NC and Pt@C in (a) 0.5 M H_2SO_4, (b) 1.0 M KOH, and (c) 1.0 M PBS, respectively.

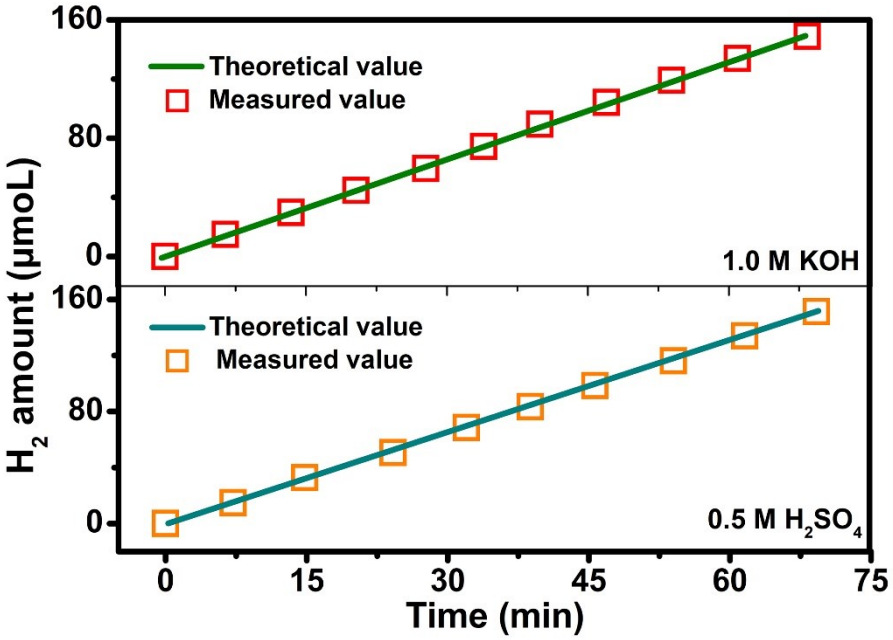

Fig. S24 Faraday efficiency of VN/Co-NC during HER in both 1.0 M KOH and 0.5 M H_2SO_4.

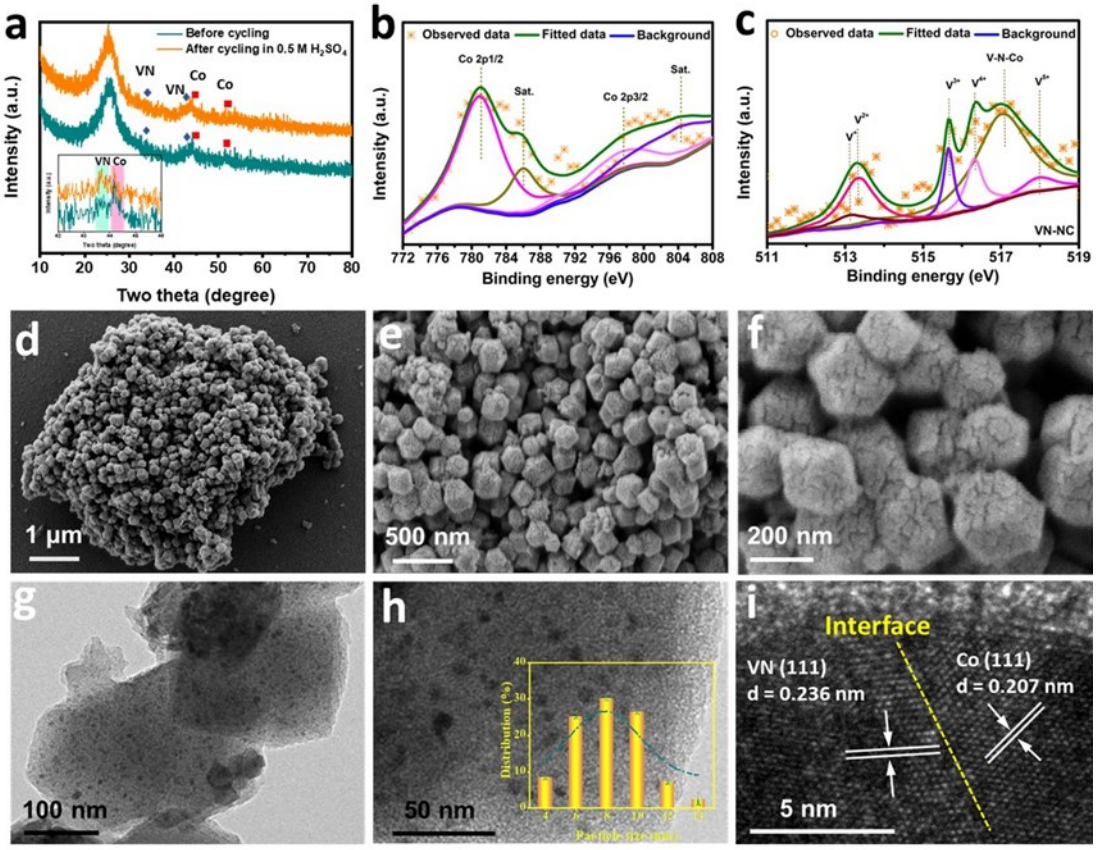

Fig. S25 VN/Co-NC electrocatalyst after 1000 cycles in 0.5 M H_2SO_4: (a) XRD patterns; high-resolution (b) Co 2p and (c) V 2p XPS spectra; (d–f) FESEM images; (g, h) TEM images and (i) HRTEM image. Inset in (h): the particle size distribution.

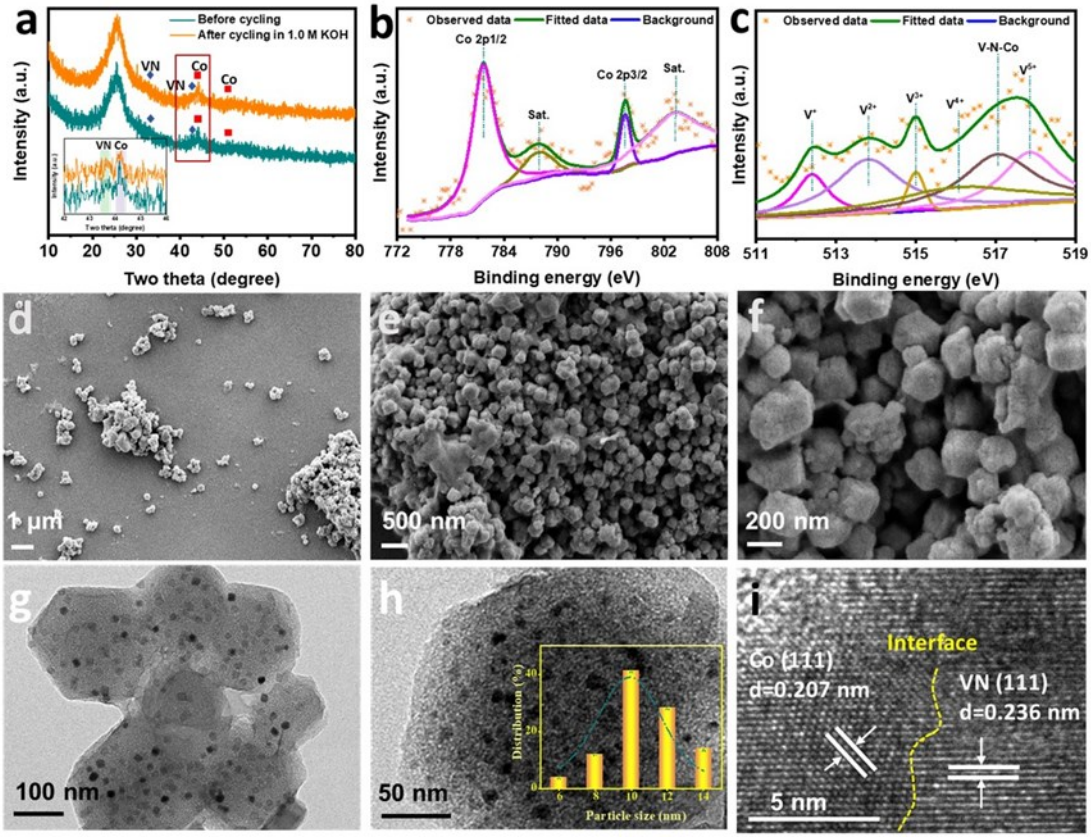

Fig. S26 VN/Co-NC electrocatalyst after 1000 cycles in 0.5 M H_2SO_4: (a) XRD patterns; high-resolution (b) Co 2p and (c) V 2p XPS spectra; (d–f) FESEM images; (g, h) TEM images and (i) HRTEM image. Inset in (h): the particle size distribution.

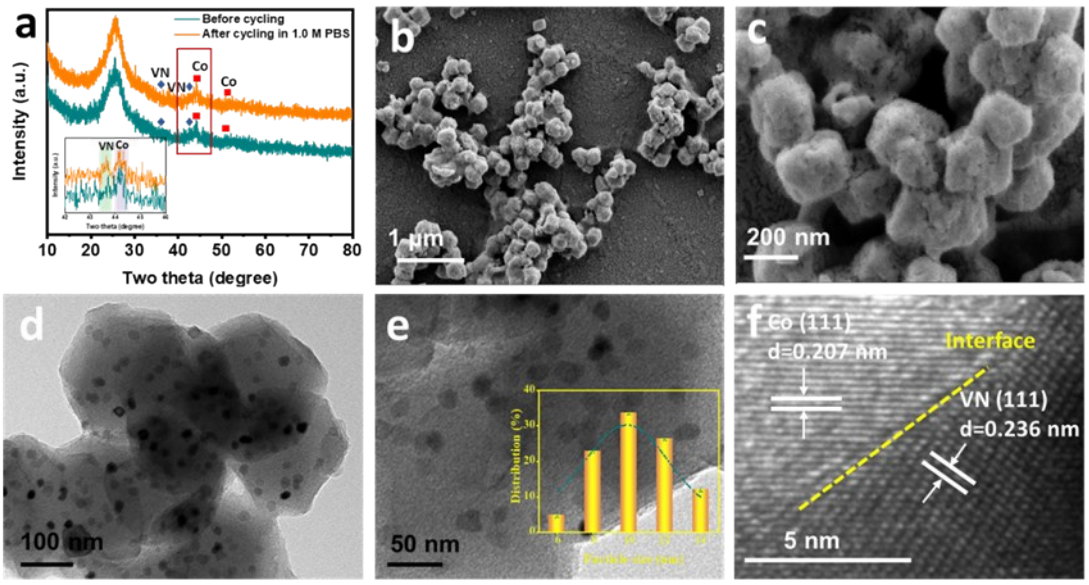

Fig. S27 VN/Co-NC electrocatalyst after 1000 cycles in 1.0 M PBS: (a) XRD patterns; (b, c) FESEM images; (d, e) TEM images and (f) HRTEM image. Inset in (e): the particle size distribution.

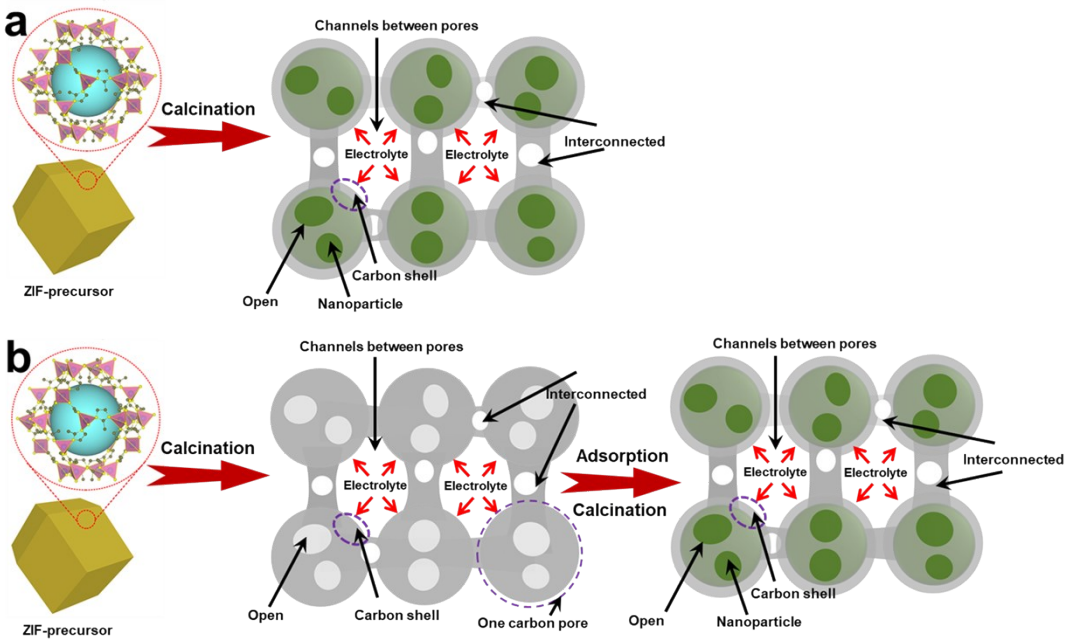

Fig. S28. The schematic illustration for the synthesis of MOF-derived porous carbon-encapsulated metal nanoparticles nanohybrid by (a) one-pot calcination and (b) multiple-step treatment.

MOFs have been demonstrated as an ideal platform to derive the nanohybrids consisting of transition metal (TM) nanoparticles encapsulated by nitrogen-doped porous carbon (TM@NC).[S101-S103] Generally, two ways were reported to construct above nanohybrids.

Taking Zn/Co-based zeolite imidazolate framework (ZIF) as an example, the first way is to directly pyrolyze Co-based ZIF (ZIF-67) under an inert atmosphere, during which the Co species liberated from ZIF-67 were reduced and migrated to form Co nanoparticles while the ligands were *in-situ* converted to N-doped porous carbon, generating the final hybrid structure constructed by encapsulating nanoparticles within the N-doped porous carbon (Fig. S28a).

The second way is to adopt a multiple-step treatment (Fig. S28). Firstly, the N-doped porous carbon framework was achieved by calcinating the Zn-ZIF (ZIF-8) at high temperature (usually over 800 ^{o}C) under an inert atmosphere, during which the nano-sized Zn species were thermally evaporated while the ligands were *in-situ* converted to the N-doped porous carbon.[S103, S104] As an alternative, the N-doped porous carbon framework could also be obtained by acid leaching of ZIF-67-derived Co@NC in the high-concentration acid solution (e.g. 3.0 M H_2SO_4).[S105, S106] This result indicated that the NC has an open porous structure and the encapsulated Co nanoparticles are easily corroded by a high-concentration acid solution. After that, the as-obtained N-doped porous carbon skeleton was deliberately selected as the host to isolate metal sources guest within pores usually by a dual-solvent method. Finally, upon further annealing towards the metal species-adsorbed porous carbon skeleton at high temperature, the metal nanoparticles were *in-situ* formed by a thermal reduction accompanied with atomic short diffusion, and most of them were uniformly encapsulated within the interconnected carbon pores.[S107]

In our case, after the first calcination towards ZIF-8, the achieved average carbon pore size was around 2 nm. However, after the adsorption of Co/V-ions followed by the second calcination, the average particle size was around 8 nm, implying the concurrent enlargement of the pore size. This may be due to the catalytic effect of Co species towards carbon matrix.

Specifically, the presence of Co may cleave and dissociate the C-N/C-C bonds, and thus promote the graphitization of ZIF-8-derived carbon by atomic reconstruction,[S109, S111] resulting in the intimate coupling between the carbon shell and nanoparticle.

No matter the first way or the second way, the surface feature of ZIF-derived N-doped porous carbon skeleton is quite similar. Many hierarchical pores with open feature were created and interconnected in both N-doped carbon skeleton.[S108-S111] This feature could also be supported by the following comparative study.

Herein, two kinds of ZIF-67-derived Co@NC by one-pot calcination and multiple treatment mentioned above were synthesized, respectively. XRD characterization indicated that the obtained products have a similar phase composition (Fig. S29). Then, the as-synthesized Co@NC composites were evaluated as HER electrocatalyst. After the cycled LSV for 1000 times in 0.5 M H_2SO_4 solution, the ICP results indicated that ~6.5 wt% and ~7.0 wt% of Co were dissolved in solution for the one-pot- and multiple-step-prepared Co@NC composites, respectively (Table S10). The slight dissolution of Co as well as the quite closed dissolution values for these two kinds of Co@NC strongly illustrated the open features of porous carbon and their similar HER behavior. Note that because the most nanoparticles were protected by the carbon shell and chemically bonded with N at the hetero-interface, the chemical stability of Co was significantly improved, and thus showing promising as one advanced HER electrocatalyst and being extensively studied.

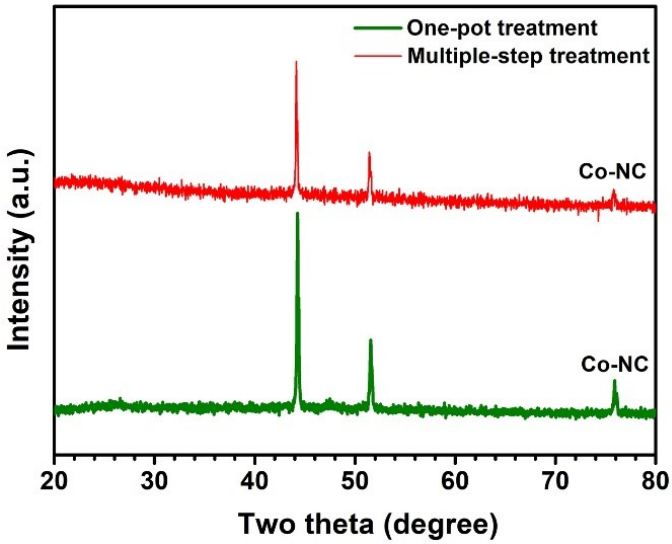

Fig. S29. XRD patterns of Co-NC composites prepared by one-pot treatment and multiple-step treatment.

Based on the above analysis and the experimental results, we may conclude that the carbon skeletons derived from the first and the second way have a similar structure and property and thus they exhibited a similar HER behavior. We also would like to clarify the structure and composition of the hybrid catalyst as following: (i) the porous within the carbon skeleton were open and interconnected; (ii) the nanoparticle and carbon shell was intimately coupled.

According to the structure features of the carbon skeleton, two parts are believed to be accessible to the electrolyte for the ZIF-derived VN/Co@NC. One is the nanoparticle-coupled carbon shells, where the electrolyte can penetrate to the channels or chinks between the pores, and then contact with the nanoparticle-coupled carbon shells. The other is the small parts of Co located at the open position of the carbon shells (Fig. S28). With regarding to these two possible active sites, previous theoretical calculations confirmed that the active site during HER was the metal nanoparticle-coupled carbon shells rather than the naked Co.[S112- S115]

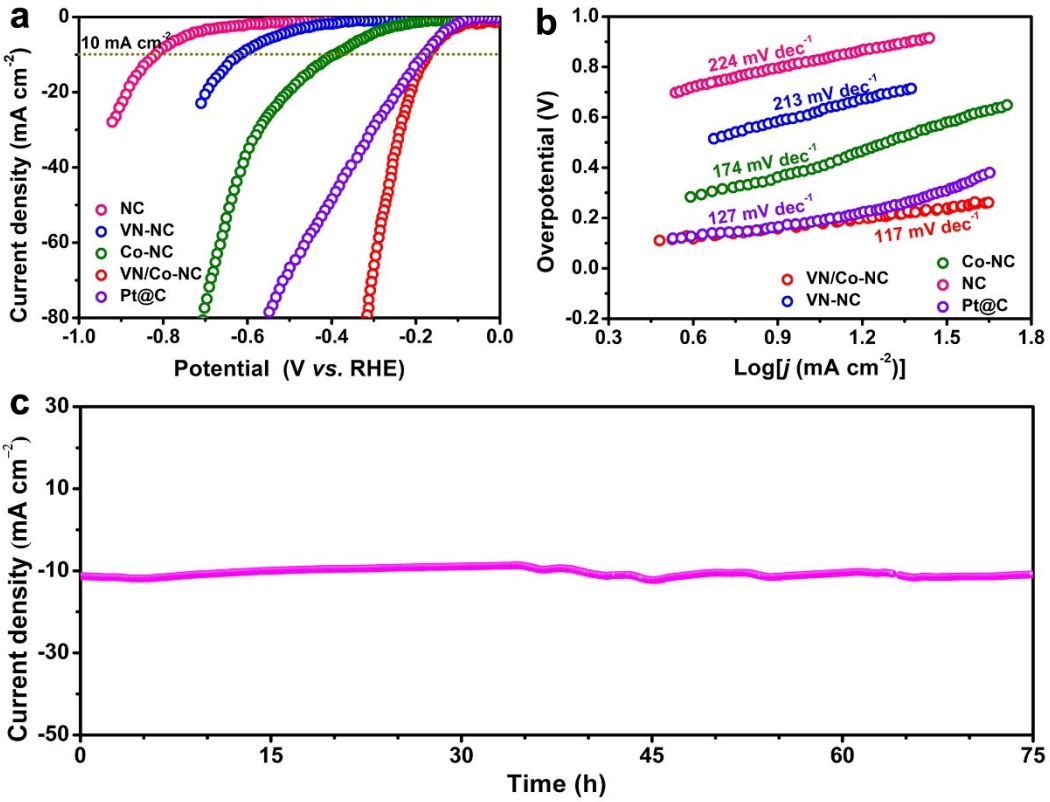

Fig. S30 (a) LSV curves and (b) Tafel slopes of VN/Co-NC, Co-NC, VN-NC, NC and Pt@C composites in 1.0 M PBS solution. (c) cycle durability of VN/Co-NC at around 10 mA cm^{-2} in 1.0 M PBS solution.

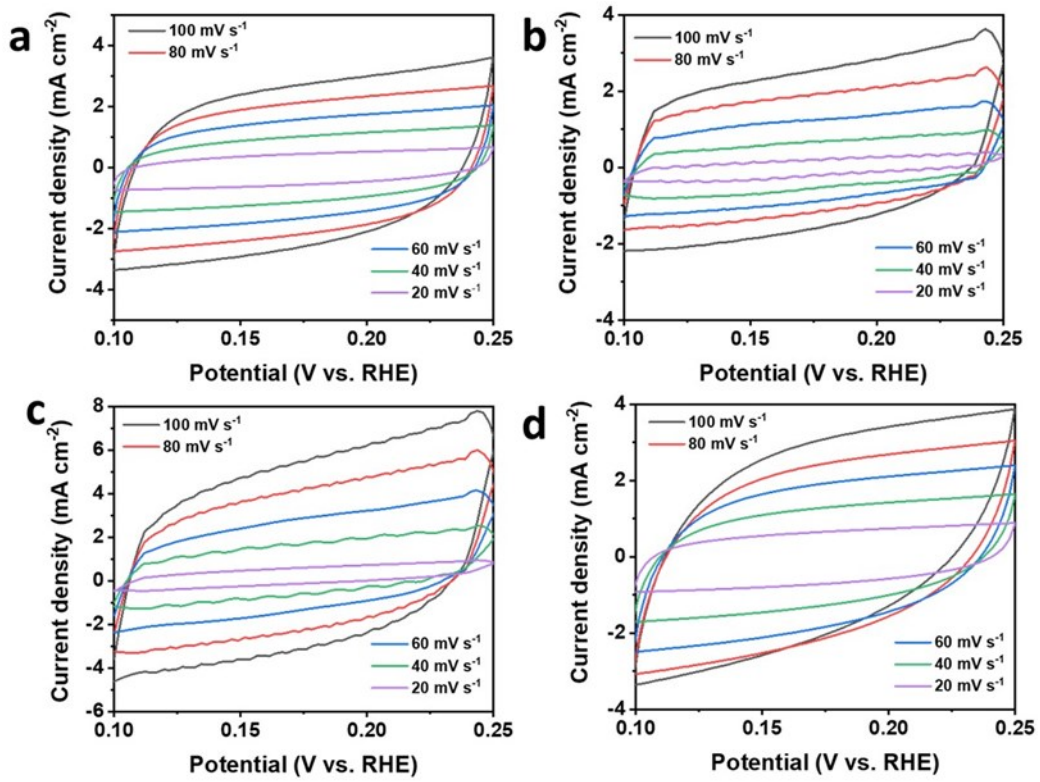

Fig. S31 CV curves at scan rates from 20, 40, 60, 80, to 100 mV s^{-1} for (a) VN/Co-NC, (b) Co-NC, (c) VN-NC, and (d) NC composites within potential ranges from 0.10 to 0.25 V in 1.0 M PBS.

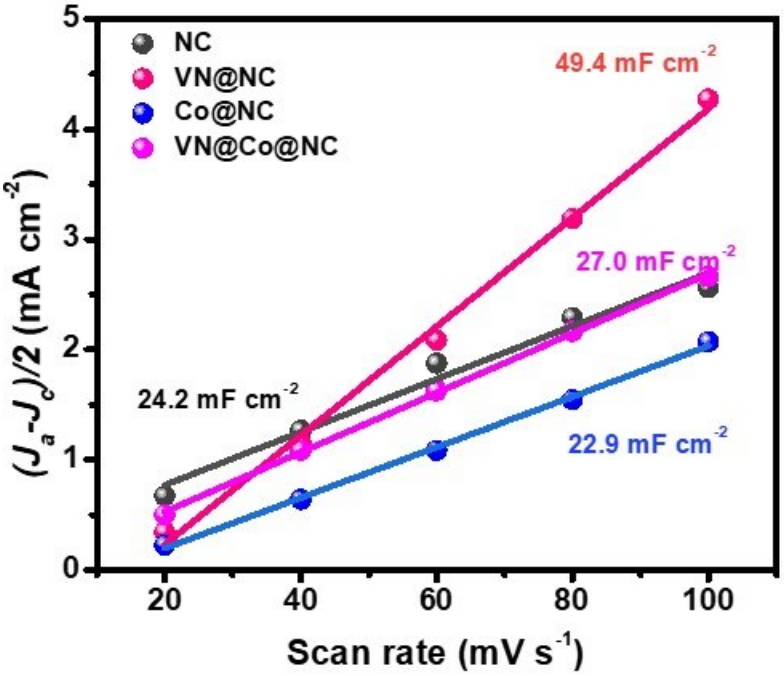

Fig. S32 C_{dl} values for VN/Co-NC, Co-NC, VN-NC, and NC composites in 1.0 M PBS electrolyte.

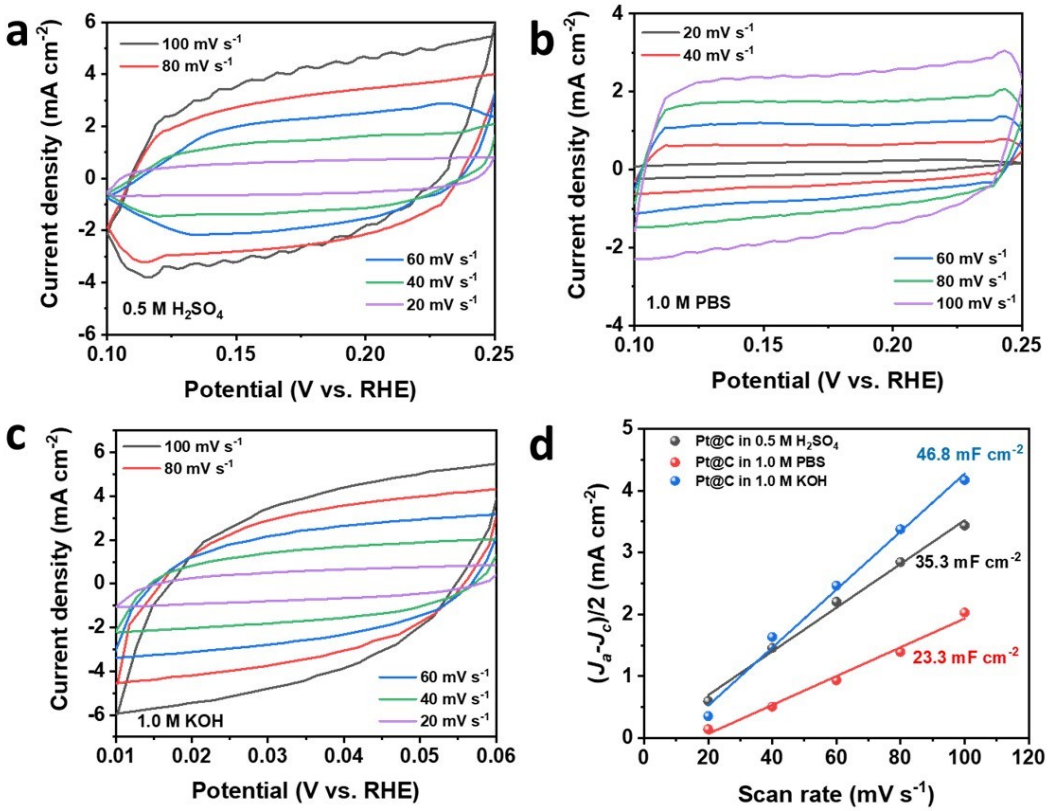

Fig. S33 CV curves at scan rates from 20, 40, 60, 80, to 100 mV s^{-1} for Pt@C from 0.10 to 0.25 V in (a) 0.5 M H_2SO_4, (b) 1.0 M PBS and (c) 1.0 M KOH, respectively; (d) C_{dl} values for Pt@C different electrolytes.

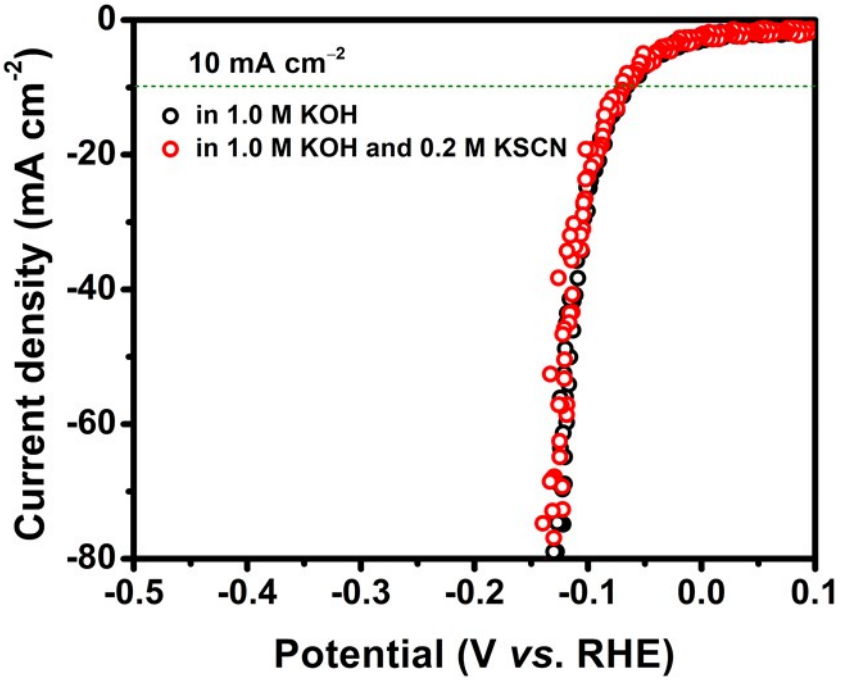

Fig. S34 Poison test: comparison of LSV curves of VN-Co/NC electrocatalyst in 1.0 M KOH solution with and without the addition of 0.2 M KSCN.

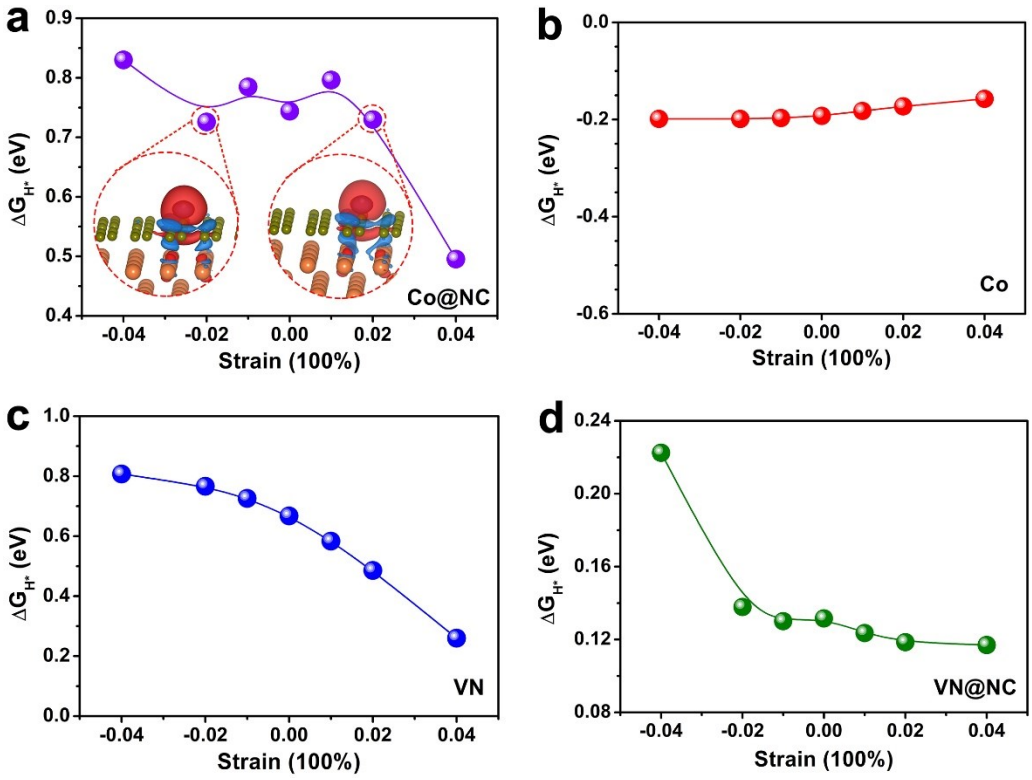

Fig. S35 Variation of ΔG_{H^*} value along with the lattice strain of (a) Co@NC, (b) Co, (c) VN and (d) VN@NC models; Inset in (a): difference charge density distributions between the substrate and H for Co@NC–H system under the lattice strain of –2% and +2%.

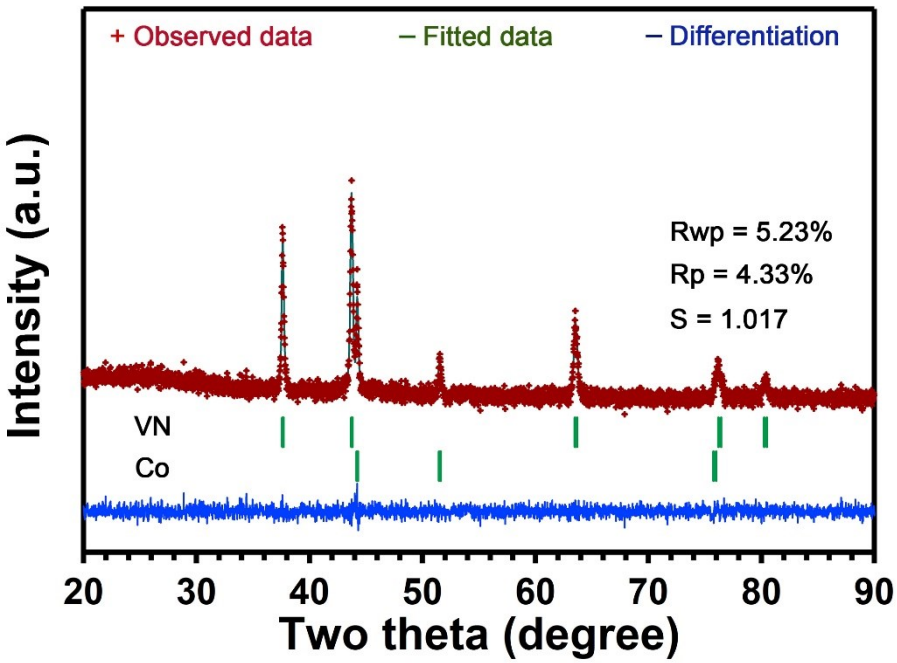

Fig. S36 Rietveld refinement for the XRD pattern of VN/Co-NC-4 composite.

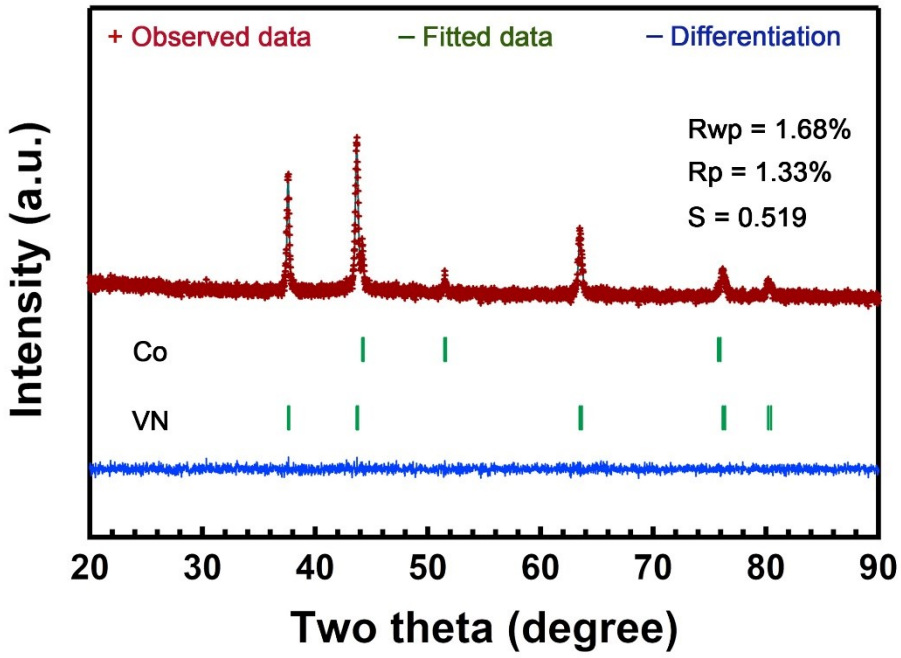

Fig. S37 Rietveld refinement for the XRD pattern of VN/Co-NC-8 composite.

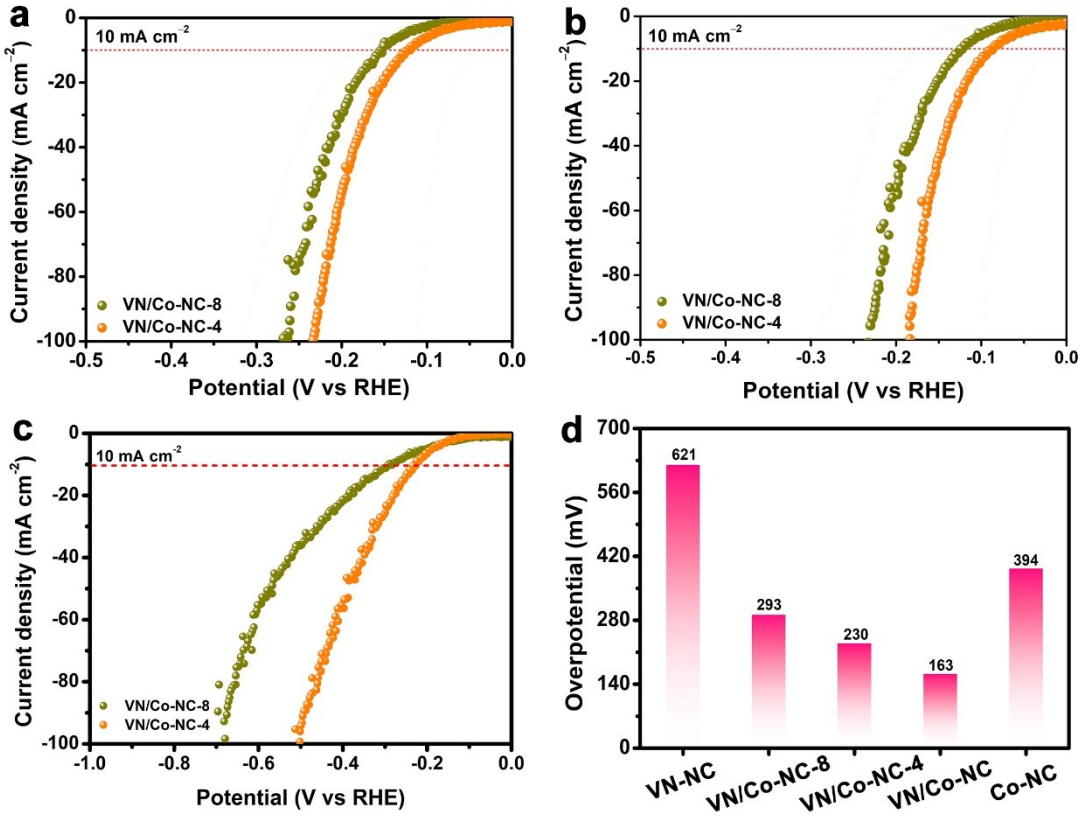

Fig. S38 LSV curves of VN/Co-NC-4 and VN/Co-NC-8 composites in (a) 1.0 M KOH, (b) 0.5 M H_2SO_4 and (c) 1.0 M PBS electrolyte. (d) Comparison of overpotentials at 10 mA cm^{-2} for VN-NC, VN/Co-NC-8, VN/Co-NC-4, VN/Co-NC, and Co-NC composites in 1.0 M PBS solution.

References

(S1) G. Zhang, P. Wang, W.-T. Lu, C.-Y. Wang, Y.-K. Li, C. Ding, J. Gu, X.-S. Zheng, F.-F. Cao, *ACS Appl. Mater. Interfaces,* 2017, **9**, 28566–28576.

(S2) L. Hu, Y. W. Hu, R. Liu, Y. C. Mao, M.-S. Balogun, Y. X. Tong, *Int. J. Hydrogen Energy,* 2019, **44**, 11402–11410.

(S3) Y. Xue, J. Li, Z. Xue, Y. Li, H. Liu, D. Li, W. Yang, Y. Li, *ACS Appl. Mater. Interfaces,* 2016, **8**, 31083–31091.

(S4) Z. Chen, Y. Ha, H. Jia, X. Yan, M. Chen, M. Liu, R. Wu, *Adv. Energy Mater.,* 2019, **9**, 1803918.

(S5) X. Zhang, H. Xu, X. Li, Y. Li, T. Yang, Y. Liang, *ACS Catal.,* 2016, **6**, 580–588.

(S6) H. Zhang, Z. Ma, J. Duan, H. Liu, G. Liu, T. Wang, K. Chang, M. Li, L. Shi, X. Meng, K. Wu, J. Ye, *ACS Nano,* 2016, **10**, 684–694.

(S7) M. Zeng, Y. Liu, F. Zhao, K. Nie, N. Han, X. Wang, W. Huang, X. Song, J. Zhong, Y. Li, *Adv. Funct. Mater.,* 2016, **26**, 4397–4404.

(S8) B. Bayatsarmadi, Y. Zheng, V. Russo, L. Ge, C. S. Casari, S. Z. Qiao, *Nanoscale,* 2016, **8**, 18507–18515.

(S9) Y. Zhao, J. Zhang, K. Li, Z. Ao, C. Wang, H. Liu, K. Sun, G. Wang, *J. Mater. Chem. A* 2016, **4**, 12818–12824.

(S10) Z. Xing, Q. Liu, W. Xing, A. M. Asiri, X. Sun, *ChemSusChem,* 2015, **8**, 1850–1855.

(S11) C. Wu, D. Liu, H. Li, J. Li, *Small,* 2018, **14**, 1704227.

(S12) H. Yang, Y. Hu, D. Huang, T. Xiong, M. Li, M.-S. Balogun, Y. Tong, *Mater. Today Chem.,* 2019, **11**, 1–7.

(S13) Y. Xu, W. Tu, B. Zhang, S. Yin, Y. Huang, M. Kraft, R. Xu, *Adv. Mater.,* 2017, **29**, 1605957.

(S14) Y. Yang, Z. Lin, S. Gao, J. Su, Z. Lun, G. Xia, J. Chen, R. Zhang, Q. Chen, *ACS Catal.,* 2017, **7**, 469–479.

(S15) M.-R. Liu, Q.-L. Hong, Q.-H. Li, Y. Du, H.-X. Zhang, S. Chen, T. Zhou, J. Zhang, *Adv. Funct. Mater.,* 2018, **28**, 1801136.

(S16) F. Yang, P. Zhao, X. Hua, W. Luo, G. Cheng, W. Xing, S. Chen, *J. Mater. Chem. A,* 2016, **4**, 16057–16063.

(S17) Z. Chen, R. Wu, Y. Liu, Y. Ha, Y. Guo, D. Sun, M. Liu, F. Fang, *Adv. Mater.* 2018, **30**, 1802011.

(S18) Y. Hou, Z. Wen, S. Cui, S. Ci, S. Mao, J. Chen, *Adv. Funct. Mater.,* 2015, **25**, 872–882.

(S19) J. Deng, P. Ren, D. Deng,X. Bao, *Angew. Chem. Int. Ed.,* 2015, **54**, 2100–2104.

(S20) H. Wang, B. Hou, Y. Yang, Q. Chen, M. Zhu, A. Thomas, Y. Liao, *Small,* 2018, **14**, 1803232.

(S21) X. Zou, X. Huang, A. Goswami, R. Silva, B. R. Sathe, E. Mikmekova, T. Asefa, *Angew. Chem. Int. Ed.,* 2014, **53**, 4372–4376.

(S22) M. Fan, Y. Zheng, A. Li, K. Li, H. Liu, Z.-A. Qiao, *Catal. Sci. Technol.,* 2018, **8**, 3695–3703.

(S23) M. Kuang, Q. Wang, P. Han, G. Zheng, *Adv. Energy Mater.* 2017, **7**, 1700193.

(S24) W. Zhao, G. Wan, C. Peng, H. Sheng, J. Wen, H. Chen, *ChemSusChem,* 2018, **11**, 3473–3479.

(S25) X. Wen, X. Yang, M. Li, L. Bai, J. Guan, *Electrochim. Acta,* 2019, **296**, 830–841.

(S26) Y. Yang, M. Luo, Y. Xing, S. Wang, W. Zhang, F. Lv, Y. Li, Y. Zhang, W. Wang, S. Guo, *Adv. Mater.*, 2018, **30**, 1706085.

(S27) R. Ge, J. Huo, T. Liao, Y. Liu, M. Zhu, Y. Li, J. Zhang, W. Li, *Appl. Catal. B: Environ.*, 2020, **260**, 118196.

(S28) W. Han, Z. Liu, Y. Pan, G. Guo, J. Zou, Y. Xia, Z. Peng, W. Li, A. Dong, *Adv. Mater.*, 2020, **32**, 2002584.

(S29) Y. Wu, J. Cai, Y. Xie, S. Niu, Y. Zang, S. Wu, Y. Liu, Z. Lu, Y. Fang, Y. Guan, X. Zheng, J. Zhu, X. Liu, G. Wang, Y. Qian, *Adv. Mater.*, 2020, **32**, 1904346.

(S30) S. Deng, Y. Zhong, Y. Zeng, Y. Wang, Z. Yao, F. Yang, S. Lin, X. Wang, X. Lu, X. Xia and J. Tu, *Adv. Mater.*, 2017, **29**, 1700748.

(S31) H. Zhu, G. Gao, M. Du, J. Zhou, K. Wang, W. Wu, X. Chen, Y. Li, P. Ma, W. Dong, F. Duan, M. Chen, G. Wu, J. Wu, H. Yang, S. Guo, *Adv. Mater.*, 2018, **30**, 1707301.

(S32) M. Zhang, J. Chen, H. Li, P. Cai, Y. Li and Z. Wen, *Nano Energy*, 2019, **61**, 576-583.

(S33) R. Boppella, J. Tan, W. Yang, J. Moon, *Adv. Funct. Mater.*, 2018, **29**, 1807976.

(S34) F. X. Ma, C. Y. Xu, F. Lyu, B. Song, S. C. Sun, Y. Y. Li, J. Lu and L. Zhen, *Adv. Sci.*, 2019, **6**, 1801490.

(S35) H. Huang, C. Yu, H. Huang, W. Guo, M. Zhang, X. Han, Q. Wei, S. Cui, X. Tan, J. Qiu, *Small Methods*, 2019, **3**, 1900259.

(S36) L. Li, L. Song, H. Xue, C. Jiang, B. Gao, H. Gong, W. Xia, X. Fan, H. Guo, T. Wang, J. He, *Carbon*, 2019, **150**, 446-454.

(S37) X. F. Lu, L. Yu, J. Zhang and X. W. D. Lou, *Adv. Mater.*, 2019, **31**, 1900699.

(S38) H. Li, M. Hu, L. Zhang, L. Huo, P. Jing, B. Liu, R. Gao, J. Zhang and B. Liu, *Adv. Funct. Mater.*, 2020, **30**, 2003198.

(S39) D. Zhao, K. Sun, W. C. Cheong, L. Zheng, C. Zhang, S. Liu, X. Cao, K. Wu, Y. Pan, Z. Zhuang, B. Hu, D. Wang, Q. Peng, C. Chen, Y. Li, *Angew Chem. Int. Ed.*, 2020, **59**, 8982-8990.

(S40) S. Chakrabartty, B. K. Barman, C. Retna Raj, *Chem. Commun.*, 2019, **55**, 4399-4402.

(S41) Q. Kang, M. Li, Z. Wang, Q. Lu, F. Gao, *Nanoscale*, 2020, **12**, 5159-5169.

(S42) Z. Huang, J. Liu, Z. Xiao, H. Fu, W. Fan, B. Xu, B. Dong, D. Liu, F. Dai, D. Sun, *Nanoscale*, 2018, **10**, 22758-22765.

(S43) S. Li, X. Jian, J. Liu, S. Guo, C. Zhou, P. Zhang, Y. Yang and L. Chen, *Inter. J. Hydrogen Energy*, 2020, **45**, 4435-4443.

(S44) H. Li, X. Qian, C. Xu, S. Huang, C. Zhu, X. Jiang, L. Shao, L. Hou, *ACS Appl. Mater. Interfaces*, 2017, **9**, 28394-28405.

(S45) L. Wang, Z. Li, K. Wang, Q. Dai, C. Lei, B. Yang, Q. Zhang, L. Lei, M. K. H. Leung, Y. Hou, *Nano Energy*, 2020, **74**, 104850.

(S46) Z. Pu, S. Wei, Z. Chen and S. Mu, *Appl. Catal. B: Environ.*, 2016, **196**, 193-198.

(S47) Z. Huang, B. Xu, Z. Li, J. Ren, H. Mei, Z. Liu, D. Xie, H. Zhang, F. Dai, R. Wang, D. Sun, *Small*, 2020, **16**, 2004231.

(S48) H. Zheng, X. Li, N. Xu, X. Wang, C. Sun, Z. Su, *ACS Omega*, 2019, **4**, 10347-10353.

(S49) P. Cheng, C. Yuan, Q. Zhou, X. Hu, J. Li, X. Lin, X. Wang, M. Jin, L. Shui, X. Gao, R. Nötzel, G. Zhou, Z. Zhang, J. Liu, *J. Phy. Chem. C*, 2019, **123**, 5833-5839.

(S50) H. Li, X. Zhao, H. Liu, S. Chen, X. Yang, C. Lv, H. Zhang, X. She, D. Yang, *Small*, 2018, **14**, 1802824.

(S51) X. Li, L. Xiao, L. Zhou, Q. Xu, J. Weng, J. Xu and B. Liu, *Angew. Chem. Int. Ed*., 2020, **59**, 21106-21113.

(S52) Y. K. Li, G. Zhang, H. Huang, W. T. Lu, F. F. Cao and Z. G. Shao, *Small*, 2020, **16**, 2005184.

(S53) Y. Li, X. Tan, H. Tan, H. Ren, S. Chen, W. Yang, S. C. Smith and C. Zhao, *Energy Environ. Sci*., 2020, **13**, 1799-1807.

(S54) T. Liu, P. Diao, Z. Lin and H. Wang, *Nano Energy*, **2020**, 74, 104787.

(S55) Y. Ma, G. Zhou, Z. Liu, L. Xu, D. Sun and Y. Tang, *Nanoscale*, 2020, **12**, 14733-14738.

(S56) W. Chen, J. Gu, Y. Du, F. Song, F. Bu, J. Li, Y. Yuan, R. Luo, Q. Liu and D. Zhang, *Adv. Funct. Mater*., 2020, **30**, 202000551.

(S57) A. B. Laursen, K. R. Patraju, M. J. Whitaker, M. Retuerto, T. Sarkar, N. Yao, K. V. Ramanujachary, M. Greenblatt and G. C. Dismukes, *Energy Environ. Sci.*, 2015, **8**, 1027-1034.

(S58) B. Ma, Z. Yang, Y. Chen and Z. Yuan, *Nano Res.*, 2018, **12**, 375-380.

(S59) X. Zhao, Z. Zhang, X. Cao, J. Hu, X. Wu, A. Y. R. Ng, G.-P. Lu and Z. Chen, *Appl. Catal. B: Environ.*, 2020, **260**, 118156.

(S60) V. Q. Bui, A. Kumar, H. T. D. Bui, J. Lee, Y. Hwang, H. M. Le, Y. Kawazoe and H. Lee, *Chem. Mate*r., 2020, **32**, 9591-9601.

(S61) X. Mu, J. Gu, F. Feng, Z. Xiao, C. Chen, S. Liu and S. Mu, *Adv. Sci*., 2021, *8*, 2002341.

(S62) H. Park, E. Lee, M. Lei, H. Joo, S. Coh and B. P. T. Fokwa, *Adv. Mater*., 2020, **32**, 2000855.

(S63) C. Jian, W. Hong, Q. Cai, J. Li and W. Liu, *Appl. Catal. B: Environ*., 2020, **266**, 118649.

(S64) J. F. Callejas, J. M. McEnaney, C. G. Read, J. C. Crompton, A. J. Biacchi, E. J. Popczun, T. R. Gordon, N. A. Lewis and R. E. Schaak, *ACS Nano*, 2014, **8**, 11101-11107.

(S65) E. J. Popczun, J. R. McKone, C. G. Read, A. J. Biacchi, A. M. Wiltrout, N. S. Lewis and R. E. Schaak, *J. Am. Chem. Soc.*, 2013, **135**, 9267-9270.

(S66) J. F. Callejas, C. G. Read, E. J. Popczun, J. M. McEnaney and R. E. Schaak, *Chem. Mater.*, 2015, **27**, 3769-3774.

(S67) J.-S. Moon, J.-H. Jang, E.-G. Kim, Y.-H. Chung, S. J. Yoo and Y.-K. Lee, *J. Catal.*, 2015, **326**, 92-99.

(S68) S. Anantharaj, J. Kennedy and S. Kundu, *ACS Appl. Mater. Interfaces*, 2017, **9**, 8714-8728.

(S69) D. Cao, H. Xu and D. Cheng, *Adv. Energy Mater*., 2020, **10**, 201903038.

(S70) M. Asnavandi, B. H. R. Suryanto, W. Yang, X. Bo and C. Zhao, *ACS Sustain. Chem. Eng*., 2018, **6**, 2866-2871.

(S71) P. Cheng, C. Yuan, Q. Zhou, X. Hu, J. Li, X. Lin, X. Wang, M. Jin, L. Shui, X. Gao, R. Nötzel, G. Zhou, Z. Zhang and J. Liu, *J. Phys. Chem. C*, 2019, **123**, 5833-5839.

(S72) A. Irshad and N. Munichandraiah, *ACS Appl. Mater. Interfaces*, 2017, **9**, 19746-19755.

(S73) R.-Q. Li, P. Hu, M. Miao, Y. Li, X.-F. Jiang, Q. Wu, Z. Meng, Z. Hu, Y. Bando and X.-B. Wang, *J. Mater. Chem. A*, 2018, **6**, 24767-24772.

(S74) J. Liu, D. Zhu, T. Ling, A. Vasileff and S.-Z. Qiao, *Nano Energy*, 2017, **40**, 264-273.

(S75) X. Xie, M. Song, L. Wang, M. H. Engelhard, L. Luo, A. Miller, Y. Zhang, L. Du, H. Pan, Z. Nie, Y. Chu, L. Estevez, Z. Wei, H. Liu, C. Wang, D. Li and Y. Shao, *ACS Catal*., 2019, **9**, 8712-8718.

(S76) H. Li, P. Wen, D. S. Itanze, M. W. Kim, S. Adhikari, C. Lu, L. Jiang, Y. Qiu, S. M. Geyer, *Adv. Mater.*, 2019, **31**, 1900813.

(S77) Q. Zhou, Z. Shen, C. Zhu, J. Li, Z. Ding, P. Wang, F. Pan, Z. Zhang, H. Ma, S. Wang, H. Zhang, *Adv. Mater.*, 2018, **30**, 1800140.

(S78) Y. Tan, H. Wang, P. Liu, Y. Shen, C. Cheng, A. Hirata, T. Fujita, Z. Tang, M. Chen, *Energy Environ. Sci.*, 2016, **9**, 2257-2261.

(S79) Y.-J. Ko, J.-M. Cho, I. Kim, D. S. Jeong, K.-S. Lee, J.-K. Park, Y.-J. Baik, H.-J. Choi, W.-S. Lee, *Appl. Catal. B: Environ.*, 2017, **203**, 684-691.

(S80) S. Chakrabartty, D. Sahu, C. R. Raj, *ACS Appl. Energy Mater.*, 2020, **3**, 2811-2820.

(S81) J. Kibsgaard, T. F. Jaramillo, *Angew Chem. Int. Ed .,* 2014, **53**, 14433-14437.

(S82) Q. Li, C. Han, X. Ma, D. Wang, Z. Xing, X. Yang, *J. Mater. Chem. A*, 2017, **5**, 17856-17861.

(S83) S. Geng, H. Liu, W. Yang,d Y. S. Yu, *Chemistry*, 2018, **24**, 19075-19080.

(S84) K. Li, Y. Li, Y. Wang, J. Ge, C. Liu and W. Xing, *Energy Environ. Sci.*, 2018, **11**, 1232-1239.

(S85) H. Fei, J. Dong, M. J. Arellano-Jimenez, G. Ye, N. Dong Kim, E. L. Samuel, Z. Peng, Z. Zhu, F. Qin, J. Bao, M. J. Yacaman, P. M. Ajayan, D. Chen, J. M. Tour, *Nat. Commun.*, 2015, **6**, 8668.

(S86) G. Li, C. Fu, W. Shi, L. Jiao, J. Wu, Q. Yang, R. Saha, M. E. Kamminga, A. K. Srivastava, E. Liu, A. N. Yazdani, N. Kumar, J. Zhang, G. R. Blake, X. Liu, M. Fahlman, S. Wirth, G. Auffermann, J. Gooth, S. Parkin, V. Madhavan, X. Feng, Y. Sun, C. Felser, *Angew Chem. Int. Ed.,* 2019, **58**, 13107-13112.

(S87) T. Ling, D. Y. Yan, H. Wang, Y. Jiao, Z. Hu, Y. Zheng, L. Zheng, J. Mao, H. Liu, X. W. Du, M. Jaroniec and S. Z. Qiao, *Nat Commun*, 2017, **8**, 1509.

(S88) J. Zhang, T. Wang, P. Liu, S. Liu, R. Dong, X. Zhuang, M. Chen, X. Feng, *Energy Environ. Sci.*, 2016, **9**, 2789-2793.

(S89) A. B. Laursen, K. R. Patraju, M. J. Whitaker, M. Retuerto, T. Sarkar, N. Yao, K. V. Ramanujachary, M. Greenblatt and G. C. Dismukes, *Energy Environ. Sci.*, 2015, **8**, 1027-1034.

(S90) J. Mahmood, F. Li, S. M. Jung, M. S. Okyay, I. Ahmad, S. J. Kim, N. Park, H. Y. Jeong, J. B. Baek, *Nat. Nanotechnol.*, 2017, **12**, 441-446.

(S91) J. Zhang, Z. Zhang, Y. Ji, J. Yang, K. Fan, X. Ma, C. Wang, R. Shu, Y. Chen, *Appl. Catal. B: Environ.*, 2021, **282**, 119609.

(S92) H. Fu, Y. Gu, A. Wu, Y. Jiao, H. Zheng, X. Wang, Y. Xie, L. Wang, C. Tian, *Angew Chem Int Ed Engl*, 2020, DOI: 10.1002/anie.202016102.

(S93) P. Zhai, Y. Zhang, Y. Wu, J. Gao, B. Zhang, S. Cao, Y. Zhang, Z. Li, L. Sun, J. Hou, *Nat. Commun.*, 2020, **11**, 5462.

(S94) L. Yu, L. Wu, S. Song, B. McElhenny, F. Zhang, S. Chen, Z. Ren, *ACS Energy Letters*, 2020, **5**, 2681-2689.

(S95) L. Tao, M. Huang, S. Guo, Q. Wang, M. Li, X. Xiao, G. Cao, Y. Shao, Y. Shen, Y. Fu, M. Wang, *Appl. Catal. B: Environ.*, 2019, **254**, 424-431.

(S96) X. Gao, Y. Chen, T. Sun, J. Huang, W. Zhang, Q. Wang, R. Cao, *Energy Environ. Sci.*, 2020, **13**, 174-182.

(S97) S. Li, S. Sirisomboonchai, X. An, X. Ma, P. Li, L. Ling, X. Hao, A. Abudula, G. Guan, *Nanoscale*, 2020, **12**, 6810-6820.

(S98) X. Ren, D. Wu, R. Ge, X. Sun, H. Ma, T. Yan, Y. Zhang, B. Du, Q. Wei, L. Chen, *Nano Research*, 2018, **11**, 2024-2033.

(S99) K. Jiang, B. Liu, M. Luo, S. Ning, M. Peng, Y. Zhao, Y. R. Lu, T. S. Chan, F. M. F. de Groot and Y. Tan, *Nat. Commun.*, 2019, **10**, 1743.

(S100) B. L. Deng, D. Wang, Z. Q. Jiang, J. Y. Zhang, S. Q. Shi, Z. J. Jiang, M. L. Liu, Carbon, 2018, 138, 169–178.

(S101) Z. Chen, H. Qing, K. Zhou, D. Sun and R. Wu, Prog. Mater. Sci., 2020, 108, 100618.

(S102) H. F. Wang, L. Chen, H. Pang, S. Kaskel and Q. Xu, Chem. Soc. Rev., 2020, 49, 1414-1448.

(S103) M. Zhang, Q. Dai, H. Zheng, M. Chen and L. Dai, Adv. Mater., 2018, 30, 1705431.

(S104) H. L. Jiang, B. Liu, Y. Q. Lan, K. Kuratani, T. Akita, H. Shioyama, F. Zong and Q. Xu, J. Am. Chem. Soc., 2011, 133, 11854-11857.

(S105) W. Ma, N. Wang, Y. Fan, T. Tong, X. Han and Y. Du, Chem. Eng. J., 2018, 336, 721-731.

(S106) N. L. Torad, R. R. Salunkhe, Y. Li, H. Hamoudi, M. Imura, Y. Sakka, C. C. Hu and Y. Yamauchi, Chem. Eur. J., 2014, 20, 7895-7900.

(S107) J. Z. Li, H. G. Zhang, W. Samarakoon, W. T. Shan, D. A. Cullen, S. Karakalos, M. J. Chen, D. M. Gu, K. L. More, G. F. Wang, Z. X. Feng, Z. B. Wang, G. Wu, Angew. Chem. Int. Ed., 2019, 58, 18971–18980.

(S108) W. Zhang, X. Jiang, X. Wang, Y. V. Kaneti, Y. Chen, J. Liu, J. S. Jiang, Y. Yamauchi and M. Hu, Angew. Chem. Int. Ed., 2017, 56, 8435-8440.

(S109) F. Wang, L. Zhu, Y. Pan, Z. Li, P. Yang, M. Song, Z. Gao, Q. Fang, M. Xue and S. Qiu, Inorg. Chem. Front., 2019, 6, 32-39.

(S110) A. I. Douka, Y. Xu, H. Yang, S. Zaman, Y. Yan, H. Liu, M. A. Salam and B. Y. Xia, Adv. Mater., 2020, 32, 2002170.

(S111) X. Ma, X. Hong, L. He, L. Xu, Y. Zhang, Z. Zhu, X. Pan, J. Zhu and L. Mai, ACS Appl. Mater. Interfaces, 2019, 11, 948-956.

(S112) Y. Yang, Z. Lun, G. Xia, F. Zheng, M. He and Q. Chen, Energy Environ. Sci., 2015, 8, 3563-3571.

(S113) J. Su, Y. Yang, G. Xia, J. Chen, P. Jiang and Q. Chen, Nat. Commun., 2017, 8, 14969.

(S114) Y. Yang, Z. Lin, S. Gao, J. Su, Z. Lun, G. Xia, J. Chen, R. Zhang and Q. Chen, ACS Catal., 2016, 7, 469-479.

(S115) Z. Chen, R. Wu, Y. Liu, Y. Ha, Y. Guo, D. Sun, M. Liu and F. Fang, Adv. Mater., 2018, 30, 1802011.